LINE INTEGRAL REPRESENTATION OF FRINGE WAVES FOR PERFECTLY CONDUCTING AND IMPEDANCE SURFACES

A THESIS SUBMITTED TO

THE GRADUATE SCHOOL OF NATURAL AND APPLIED

SCIENCES OF

ÇANKAYA UNIVERSITY

BY

HÜSNÜ DENİZ BAŞDEMİR

IN PARTIAL FULFILLMENT OF THE REQUIREMENTS FOR THE

DEGREE OF

DOCTOR OF PHILOSOPHY

IN

THE DEPARTMENT OF

ELECTRONIC AND COMMUNICATION ENGINEERING

MAY 2014

Title of the Thesis : **Line Integral Representation of Fringe Waves for Perfectly Conducting and Impedance Surfaces**
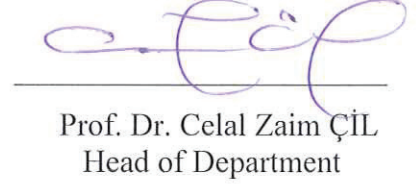
Submitted by **Hüsnü Deniz BAŞDEMİR**

Approval of the Graduate School of Natural and Applied Sciences, Çankaya University

Prof. Dr. Taner ALTUNOK
Director

I certify that this thesis satisfies all the requirements as a thesis for the degree of Doctor of Philosophy.

Prof. Dr. Celal Zaim ÇİL
Head of Department

This is to certify that we have read this thesis and that in our opinion it is fully adequate, in scope and quality, as a thesis for the degree of Doctor of Philosophy.

Prof. Dr. Yusuf Ziya UMUL
Supervisor

Examination Date :   22.05.2014

Examining Committee Members

Prof. Dr. Halil Tanyer EYYUBOĞLU	(Çankaya Univ.)	
Prof. Dr. Yusuf Ziya UMUL	(Çankaya Univ.)	
Prof. Dr. Gülbin DURAL	(METU)	
Assist. Prof. Dr. Uğur YALÇIN	(Uludağ Univ.)	
Assist. Prof. Dr. Emre SERMUTLU	(Çankaya Univ.)	

STATEMENT OF NON-PLAGIARISM PAGE

I hereby declare that all information in this document has been obtained and presented in accordance with academic rules and ethical conduct. I also declare that, as required by these rules and conduct, I have fully cited and referenced all material and results that are not original to this work.

Name, Last Name: Hüsnü Deniz BAŞDEMİR

Signature :

Date : 22.05.2014

ABSTRACT

**LINE INTEGRAL REPRESENTATION OF FRINGE WAVES FOR
PERFECTLY CONDUCTING AND IMPEDANCE SURFACES**

BAŞDEMİR, Hüsnü Deniz

Ph.D., Department of Electronic and Communication Engineering

Supervisor: Prof. Dr. Yusuf Ziya UMUL

May 2014, 63 pages

In this thesis, surface diffraction was investigated for perfectly conducting and impedance cylinders. Moreover, the line integral representations of fringe fields were derived analytically and generalized with using the unit vectors of related edge contours. Hence, the method of physical theory of diffraction was improved with reducing the scattering surface integral to line integral. The derived expressions were applied to perfectly conducting parabolic reflector geometry for investigation of exact diffracted fields. In addition, uniform expressions of scalar fringe waves which are based on the physical theory of diffraction method are derived for an impedance half-plane. The asymptotic and uniform expressions were compared for the impedance half-plane geometry. All these mentioned fields were plotted and analyzed numerically.

Keywords: Surface Diffraction, Edge Diffraction, Fringe Waves.

ÖZ

MÜKEMMEL İLETKEN VE EMPEDANS YÜZEYLER İÇİN SAÇAK ALANLARININ ÇİZGİ İNTEGRAL GÖSTERİMİ

BAŞDEMİR, Hüsnü Deniz

Doktora, Elektronik ve Haberleşme Mühendisliği Anabilim Dalı

Tez Yöneticisi: Prof. Dr. Yusuf Ziya UMUL

Mayıs 2014, 63 sayfa

Bu tezde, mükemmel iletken ve empedans silindirler için yüzey kırınımı incelenmiştir. Dahası saçak alanlarının çizgi integral gösterimi analitik olarak türetilmiş ve kenar hattıyla alakalı birim vektörler kullanılarak genelleştirilmiştir. Böylece kırınımın fiziksel teorisi metodu saçılma yüzey integrallerinin çizgi integraline indirgenmesiyle geliştirilmiştir. Kesin kırınım alanlarının araştırılması için türetilen ifadeler mükemmel iletken parabolik yansıtıcı geometrisine uygulanmıştır. Buna ek olarak, kırınımın fiziksel teorisi metoduna dayanan sürekli saçak alanlarının ifadeleri bir empedans yarım düzlemi için türetilmiştir. Empedans yarım düzlem geometrisi için asimptotik ve sürekli cinsinden ifadeler karşılaştırılmıştır. Bahsedilen bütün alan ifadeleri çizdirilmiş ve sayısal olarak analiz edilmiştir.

Anahtar Kelimeler: Yüzey Kırınımı, Kenar Kırınımı, Saçak Alanlar.

ACKNOWLEDGEMENTS

I would like to express my sincere gratitude to Prof. Dr. Yusuf Ziya UMUL for his supervision, special guidance, suggestions, and encouragement through the development of this thesis.

It is a pleasure to express my special thanks to my family for their valuable support.

TABLE OF CONTENT

LIST OF FIGURES

FIGURES

FIGURES

LIST OF ABBREVIATIONS

PTD   Physical Theory of Diffraction
PO   Physical Optics
MTPO   Modified Theory of Physical Optics
GO   Geometrical Optics
GTD   Geometrical Theory of Diffraction
UTD   Uniform Theory of Diffraction
PEC   Perfectly Electric Conducting
PMC   Perfectly Magnetic Conducting
ILDC   Incremental Length Diffraction Coefficients
EEC   Equivalent Edge Currents
HF   High Frequency
BDW   Boundary Diffraction Wave
RCS   Radar Cross Section

CHAPTER 1

INTRODUCTION

1.1 Background

In general, wave radiation has to be analyzed by taking into account scatterers. Scatterers are finite structures. These structures reflect waves from uniform tangent planes or diffract waves from their non-uniform parts [1]. In a medium, total field consists of incident field $\left(\vec{E}_i, \vec{H}_i\right)$ and scattered field $\left(\vec{E}_s, \vec{H}_s\right)$. Incident fields are produced by a source in the absence of any scatterer. Total electric and magnetic fields can be written as

$$\vec{E}_t = \vec{E}_i + \vec{E}_s \tag{1.1}$$

and

$$\vec{H}_t = \vec{H}_i + \vec{H}_s. \tag{1.2}$$

Exact solutions of the scattered fields must satisfy the Helmholtz equation and related boundary conditions. Helmholtz equation is a differential equation that can be solved by using the method of separation of variables if the scatterer's geometry is suitable. Diffraction problems are one of the most popular investigation fields of scattering problem, solutions of which are obtained by using different methods. There are three major groups of solution methods. The first one is analytic, the second one is numerical and the last one is asymptotic methods. If the variables cannot be separated, this means that the geometry is complex and then high frequency asymptotic techniques are preferred. In this thesis work we are interested in the high frequency (HF) asymptotic techniques. The high frequency asymptotic condition is satisfied when $k\rho \gg 1$, where k is the wave number, and ρ is the distance between source and observation point. This technique deviates from two major groups which are ray-based and current-based. Geometrical optics (GO),

which is one of the ray based techniques, indicates that in the high frequency, electromagnetic waves travel like rays in the vacuum [1]. This method shows us incident and reflected fields, and these fields help us to determine the good and bad zones for the communication. However, this technique does not include diffraction phenomena. GO fields, which are directly reaching the observation point is not affected by the scatterers. However, GO does not include the diffracted fields. Geometrical theory of diffraction (GTD) [2] and its uniform version of uniform theory of diffraction (UTD) [3] are popular ray-based techniques for investigation of diffraction problems. These techniques have a problem at the caustic regions. They give infinite field values at those regions. Both current-based and integral-based techniques eliminate this problem. PO, which was suggested by McDonald is one of them [4]. It is based on the integrating current, which is induced on the scatterer's surface. Although the technique is accurate in the applications, it gives wrong diffracted fields on the edges. The second defect originates from its definition where the contribution from the shadow part is excluded. These defects were fixed in physical theory of diffraction (PTD) method, which was suggested by Ufimtsev in 1950s by defining additional correction current [5]. Ufimtsev called this current "non-uniform current", whereas the other authors called "fringe current". Scattered field consists of the composition of the uniform and non-uniform field components according to the PTD. The uniform field component is obtained by using the PO method. The non-uniform field component is the result of the fringe current which flows on the discontinuity of the scatterer [6]. Sommerfeld's exact expressions of the non-uniform currents were presented for the numerical computations by Ufimtsev [7]. PTD technique is based on this correction current. The more general form of the PTD was developed for electromagnetic edge waves by Ufimtsev [8]. PTD is based on the concept of the elementary edge waves. Grazing singularities of the PTD were eliminated by Ufimtsev for electromagnetic and acoustic wave problems [9-10]. Unfortunately, the method of PTD can be applied just for solution known problems. This originates from its definition. The new and interesting method for obtaining the exact solution of diffracted fields from perfectly electric conducting (PEC) surfaces is the modified theory of physical optics (MTPO) [11]. This technique eliminates all mentioned difficulties by defining three axioms, which are considered the scatter and

aperture surface, the angles of transmission and reflection are taken as function of the scatter and aperture coordinates, and a redefined new unit vector.

Pathak performed an UTD analysis of the scattered fields from a PEC cylinder in 1979 [12]. Asymptotic expression for the scattering by a perfectly conducting cylinder was investigated by Franz [13]. A new method for investigation of the plane wave scattering by a perfectly conducting circular cylinder near a plane surface was presented by Borghi F., Santarsiero M., Frezza F., Schettini G [14]. Asymptotic expansions of exact solutions for the scattered fields from perfectly conducting cylinder were investigated on the complex plane and critical discussions GO, PO and GTD were presented by Kouyoumjian [15]. Diffracted and reflected fields by any convex cylinder were constructed by Keller [16]. The eigen-function solution for electromagnetic scattering by the cylinder was published in 1881 [17], the parabolic cylinder in 1914 [18]. Debye obtained asymptotic approximation for the current on the illumination side of the cylinder by using the saddle point method [19]. Riblet gave the first two terms of the asymptotic expansion of the current on the illuminated part of the cylinder [20]. Wetzel published a study about the high frequency currents on the all parts of the cylinder [21]. Wait obtained the current on a parabolic cylinder in the vicinity of the shadow boundary [22]. An analytical solution was presented for the electromagnetic scattering from a dielectric cylinder by Lawrence and Sarabandi [23]. Scattering from a perfectly conducting cylindrical reflector was examined by Yalçın [24]. Physical optics integral was obtained for a cylinder by Umul at all. [25]. Plane wave scattering by a perfectly conducting circular cylinder near a plane surface was investigated by Borghi at all. [26]. Diffraction of waves generated by magnetic line source by the edges of a cylindrically curved surface with different phase impedance was presented by Büyükaksoy and Uzgören [27]. The diffracted fields from the smooth convex perfectly conducting surface and the contributions of the PO and PTD currents which are described in terms of the Fresnel function and the non-singular Pekeris functions were investigated by Michaeli with the method of PTD [28]. Equivalent surface currents were implemented in a standard general purpose PTD code by Syed and Volakis for a number of impedance and coated structures [29]. PTD was applied to a perfectly conducting cylinder to investigate the diffracted fields by Başdemir [30-31].

3

The third chapter of this thesis is allocated for investigation of the surface diffraction from PEC and impedance cylinders. The contribution of this work is in the application of the PTD method, both for impedance and PEC cylinders. Although PEC cylinder was investigated previously by us [30], according to our knowledge, there is no work in the literature about the application of the PTD to an impedance cylinder for the investigation of the surface diffraction. The PEC cylinder will be revisited for increasing the intelligibility of the applied method. Using PTD method, the fringe currents and the fringe fields will be obtained and the contributions of these related to the scattered fields and the impacts of the surface diffraction will be investigated in the third chapter.

Young first proposed the physical meaning of the scattered fields from a knife edge by the superposition of the incident and edge diffracted fields [32]. Although his valuable idea was allowed to show the interference characteristic of the scattered fields, his interpretation did not based on mathematics. Therefore, this proposal was dominated by the Fresnel's theory of diffraction. Later on, Maggi and Rubinowitz independently derived mathematical expressions for the qualitative representation of the Young's idea by using the Kirchhoff's integral formula [33-34]. The obtained line integrals are the reduction forms of the surface integrals to the line integrals and the evaluation of these integrals directly gives the edge diffracted fields. This theory provides the investigation of the diffracted fields independently from the total scattered fields. However, Ganci's works on the half plane showed that the solution of the Maggi-Rubinowitz (boundary diffraction wave, BDW) gives an approximate solution like physical optics (PO) [35-36]. Ufimtsev improved his theory with reducing his surface integrals to reduce the edge point contributions but he did it indirect and heuristic considerations [37]. Mitzner and Michaeli also used this surface to edge reduction technique independently [38-39]. The result of the Mitzner's work was formulated in terms of the incremental length diffraction coefficients (ILDC) and the Michaeli's work was formulated in terms of the equivalent edge currents (EEC) for wedge like solutions. Both approaches were compared by Knott [40]. Michaeli's expressions are finite for all directions of incidence and observation for edges. In the oblique incidence observation point is described with two different angles. The first one, β is related with the edge contour

and second one, ϕ is related with the plane of the perpendicular incidence [39]. The scattering angle β was taken different from the incident angle according to Michaeli for the case of oblique incidence. Thus, the equivalent edge currents were improved for the observation points that are out of the Keller's cone. The angle β is the function of the integral variable but he did not modify the ϕ angle. According to the equivalent edge current method of Michaeli, the angle ϕ is not a function of the integration variable. However, the angle ϕ becomes variable at the discontinuity of an edge. Because of this, at the corners, the method gives wrong diffracted fields. Umul has overcome this corner problem with defining the exact form of the equivalent edge currents by using the axioms of the modified theory of physical optics (MTPO) [41-42]. The curved surface diffraction has been studied by many researchers. The scattering of the electromagnetic fields from the curved surfaces was studied by Büyükaksoy and Uzgören [43], and also Akduman and Büyükaksoy [44]. Scattering of a line source from a cylindrical parabolic impedance reflector was investigated by Umul [45]. Scattering from a cylindrical reflector which is fed by an offset electrical line source was investigated by Yalçın [46].

In the fourth chapter of this thesis, rigorous form of the fringe field expressions will be obtained and generalized by using the unit vectors. The obtained expressions will be applied to the parabolic reflector geometry, which has the PEC boundary condition and is fed by the H-polarized magnetic line source. The method that is based on the MTPO axioms will be applied.

The half-plane problem is one of the most fundamental problems of diffraction phenomena. Exact solution of this problem was obtained for the PEC case by Sommerfeld in 1882. Ufimtsev's PTD is based on this exact solution. Non-uniform fringe fields can be obtained by the subtraction of asymptotic PO fields from asymptotic exact solutions. Similarly, uniform fringe fields can be obtained by subtraction of uniform PO fields from uniform exact solutions of the related geometry. Using the uniform fringe fields instead of the non-uniform version is more reliable. Umul pointed out after a comparison that the values used by Ufimtsev were quite large and not giving the correct results for the fringe fields [47]. According to Umul's work, approximate expressions are not valid in the transition regions.

Therefore, the solutions that are represented by the Fresnel functions must be used for the scattering problems [47]. Syed and Volakis derived PTD formulation for investigation of radar cross section (RCS) and they presented their formulation for impedance and coated structures [48]. Although PTD results for different impedance structures were presented by Syed and Volakis, fringe field expressions were not studied analytically and numerically. In addition, the work does not include the uniform version of the fringe field expressions and results were analyzed in terms of the total fields. In the literature, there are lots of applications on the diffraction analysis for impedance surfaces such as land-sea transition, solar cell panels on satellites and edges of high performance antennas [49-52].

In the fifth chapter of this thesis, uniform fringe field expressions for impedance half-plane will be investigated. Although the diffraction from a half-plane was studied by many researchers according to our knowledge, there is no study on the application of the PTD method to an impedance-half plane. Moreover, uniform expressions of fringe fields have not been examined for an impedance half-plane. It will be examined in this thesis for the first time. Additionally, uniform and non-uniform expressions will also be derived and compared numerically. Differences will be examined according to the distribution of fringe field. All these mentioned fields will be analyzed numerically in the numerical parts of the chapters by using MATLAB.

The time factor of $\exp(j\omega t)$ is assumed and suppressed throughout the thesis where ω is the angular frequency.

1.2 Objectives

The primary aim of this study is to reduce of the scattering surface integral to a line integral in order to directly obtain the edge diffracted fringe fields. Thus, the obtained integral expression is generalized for the PEC case. The derived fringe expression is used for investigation of the contribution to the scattered fields for parabolic reflector geometry. Moreover, the contribution of the diffracted fields to the scattered fields for different geometries such as half-planes and cylinders with the impedance boundary conditions is also studied. The method, which is used for this

aim is the physical theory of diffraction (PTD). The derived expressions of the fringe fields are transformed into uniform versions. In some applications, asymptotic and uniform fringe field expressions are compared. All these field expressions are analyzed numerically.

1.3 Organization of the Thesis

This thesis contains six chapters. All the necessary information about the reduction of the scattering surface integral to line integral representation, methods used for the derivation of the fringe fields and numerical analysis of these fields can be found for different geometries.

Chapter 1 is an introduction to the history of edge diffraction and objectives of this thesis.

Chapter 2 includes an introduction of the physical optics and physical theory of diffraction technique which will be used in this thesis. In addition, line integral representation of fringe fields and generalization process are introduced.

In Chapter 3, generalized form of the fringe waves for perfectly electric conducting edge and its application of the parabolic reflector are studied.

In Chapter 4, perfect electric conducting and impedance cylinder application of the PTD in terms of the series solutions are investigated.

Chapter 5 includes the derivation of the fringe fields for an impedance half-plane and comparison of the asymptotic and uniform fringe fields.

Chapter 6 includes the conclusion part.

CHAPTER 2

CURRENT BASED TECHNIQUES

2.1 Fundamental Concept of the Current Based Techniques

The exact solutions of the scattered fields can be obtained by the solution of the Helmholtz equation for appropriate geometries. In some cases, especially for the complex geometries, solution methods can be inadequate for the Helmholtz equation. The expressions are not separated to variables because of the complexity of geometries. In this situation, high-frequency asymptotic techniques are more suitable to obtain the scattered field expressions. The current based techniques are one of the most known high frequency asymptotic techniques. The basic idea for this approximation is to define an equivalent current on the tangential plane of the scatterer object by the incident field. This approximation is valid in the high frequencies, which means that $k\rho \gg 1$ when compared with the scattering object. In this case, k is the wave number and ρ is the observation distance. Figure 1 shows the induced current on the scattering object.

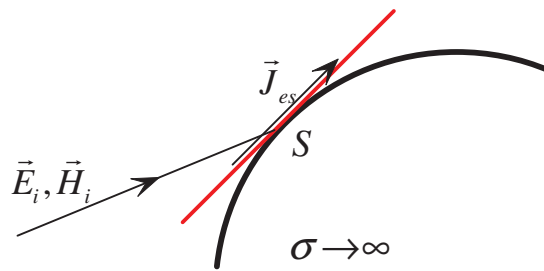**Figure 1** Induced surface current by incident wave

It can be seen from the Fig. 1 that $\vec{J}_{es}$ is the induced electric current by the incident wave. Induced current can be thought as the source of the scattered field. This current is modeled mathematically with respect to the boundary conditions of any scatterer's surface. Scattered field includes geometrical optical fields which are

incident $\left(\vec{E}_i\right)$, reflected $\left(\vec{E}_r\right)$ fields respectively and also includes diffracted fields $\left(\vec{E}_d\right)$. Examples of the current based techniques are the modified theory of physical optics (MTPO) [11], physical optics (PO) [4] and physical theory of diffraction (PTD) [5].

2.2 Physical Optics (PO)

In the high-frequency asymptotic techniques, the PO and its scalar version, called the extended Kirchhoff integral, are useful methods for investigation of the scattering phenomena. The method PO was suggested by Mcdonald in 1913 [4]. It can be a good prediction of the scattered fields for large metallic objects. Since the situations of reflection and diffraction have a local character in high-frequencies, the related approximation is valid for the problems where the size of the scatterer is sufficiently greater than the wavelength. According to this technique, induced field on the object is determined by the geometrical optics. Geometrical optics (GO) gives us the electromagnetic waves that travel in ray tubes at high frequencies. For this reason this technique is generally named as ray optics. In a homogeneous medium, energy moves along ray paths that are straight lines. We can assume the surface of the scattering object as an infinite tangential plane with respect to small wavelength according to obstacle. This surface is called geometric optic surface. The main idea is to achieve current on the scatterer. Current induced by the incident field can be written,

$$\vec{J}_{PO} = \vec{n} \times \vec{H}_t \text{ , in the lit region} \tag{2.1}$$

and

$$\vec{J}_{PO} = 0 \text{ , in the shadow region} \tag{2.2}$$

where $\vec{n}$ is the unit normal vector which is outward from the illuminated part of the scatterer as shown in Fig. 2. Keep in mind that PEC case is considered. $\vec{H}_t$ is the total magnetic field intensity. It is defined on the scatterer's surface. Since PO takes the reflected fields as GO fields, the total field on the surface is twice of the incident field.

9
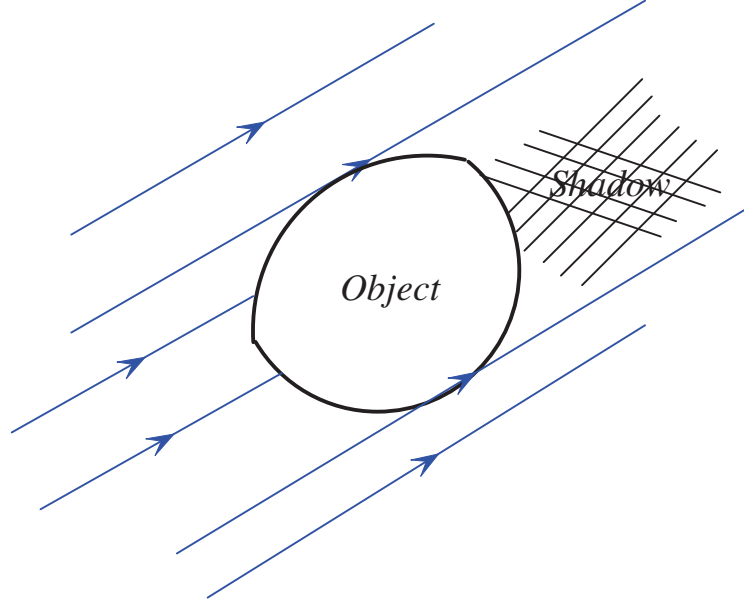
Figure 2 Physical optics lit and shadow regions

In the far field total scattering PO field can be found

$$\vec{E}_s^{PO} \cong -j\omega\vec{A} \tag{2.3}$$

from the Eq. (2.3). $\vec{A}$ shows the magnetic vector potential. For finding the magnetic vector potential, physical optics scattering integral is written as

$$\vec{A} = \frac{\mu_0}{4\pi} \iint_{S'} \vec{J}_{PO} G ds' \tag{2.4}$$

where the integral is defined over the scatterer's surface. The term G is the free space Green's function and equal to $\dfrac{\exp(-jkR)}{R}$ where minus sign in the exponential term corresponding the waves is propagating in the outward direction, and R is the distance between the source and observation point. Green's function includes the phase and magnitude variations information away from the source. The method PO has two important defects. The first one is the incorrect contribution of edge diffraction to the scattering integral. This defect was eliminated by Umul by using modified version of the surface currents [11]. He obtained the exact solution of the edge diffracted waves for PEC half-plane by using this method. Later on, this method was extended for wedge problem by Umul [53]. The second defect of the PO method is the absence of the shadow surface currents. These are the results of the definition of PO method. The PO approximation is based on the GO and GO predicts zero field

in the shadow region. Thus, the surface currents on this part of scatterer are taken as zero. For this reason, it is not possible to evaluate the exact scattered fields with a wedge by using PO method since PO only takes into account the illuminated part of the scatterer and reduces the wedge problems to the half-plane. The physical theory of diffraction (PTD) was proposed by Ufimtsev to overcome this defect [5].

2.3 Physical Theory of Diffraction (PTD)

As mentioned before, it is not possible to evaluate the exact scattered fields by using the PO method because of its definition. The PO current limited only the illuminated part of the scatterer, so it leads to wrong diffracted field contribution to the scattered field. In this situation, PO reduces the wedge like geometries to the half-plane problem. For this reason, a method called physical theory of diffraction was introduced by Ufimtsev in 1950's [5]. The aim of the method is to obtain the exact wedge diffracted waves by using the exact solution. When Ufimtsev was improving the PO technique, he was aware of the Sommerfeld's exact wedge solution [54]. The fundamental idea of Ufimtsev's concept is to divide the induced current into two components. This total current can be thought as the source of the scattered field. It can be defined as

$$\vec{J}_t = \vec{J}_{uniform} + \vec{J}_{nonuniform} \qquad (2.5)$$

in terms of the uniform and non-uniform currents. First part, $\vec{J}_{uniform}$, is called the uniform part of the current. This part is obtained from the PO. PO current is described on the lit region of the scatterer's tangential surface which is called the geometric optic surface. PO approximation is based on the GO fields. Since GO predicts zero field in the shadow region, the shadow current is taken as zero by the PO method. The incident wave shows equal distribution over the tangential plane. Its amplitude is constant and its phase is a linear function of the plane coordinates. Because of this it is named as the uniform component. The currents which are induced over the tangential plane of the scatterer are defined by taking into account the surface boundary conditions. The PTD method is valid for both acoustic and electromagnetic surfaces. The relation between the acoustic and electromagnetic

surfaces has to be described. On the acoustically soft plane, total field on the scatterer is equal to zero and can be written as

$$u_t\big|_{soft} = 0 \qquad\qquad (2.6)$$

but its normal derivative is different from zero. On the acoustically hard plane, total field can be given as

$$u_t\big|_{hard} = 2u_i \qquad\qquad (2.7)$$

but its normal derivative is equal to zero on the surface. On a PEC surface the tangential component of the electric field intensity is equal to zero. If the electric field polarization is parallel to the edge of the scatterer, this time surface is called perfectly magnetic conducting (PMC) surface. These conditions tell us for electromagnetic boundary conditions in the acoustically soft plane, tangential polarization of the incident electric field is different from zero but incident magnetic field is equal to zero and in the acoustically hard plane, tangential polarization of the incident electric field is equal to zero but incident magnetic polarization is different from zero. Acoustically hard plane is described as PEC surface in the electromagnetic and acoustically soft plane is described as PMC surface in the electromagnetic. The main contribution of PTD to the diffraction phenomena is the non-uniform part which is introduced by Ufimtsev. Non-uniform parts are the discontinuity of the scattering objects. In Fig. 3 the edge, smooth bending and discontinuity of curved surface are given as the examples of discontinuities.
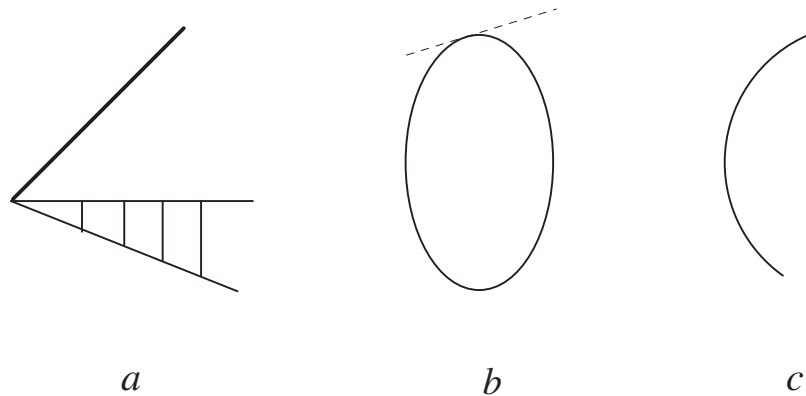

a b c

Figure 3 Different shapes where the incident field generates the non-uniform source

As seen in the Fig. 3, a is the sharp edge, b is the smooth bending and c is the discontinuity of curvature. These discontinuities are the reason of diffraction. Current induced on these discontinuities, especially on the edges, was called **fringe currents** and the fields which are radiating from these discontinuities were called **fringe fields** by the Ufimtsev [5]. Actually, Ufimtsev did not find the non-uniform currents; instead, he evaluated the non-uniform field due to the non-uniform current. Ufimtsev obtained this fringe fields subtracting PO scattered waves from the Sommerfeld's exact solution. Special feature of this technique allows us to calculate the fields which are in the shadow and the caustic regions. Although this technique is just applicable for the solution known problem, its serious contributions to the technology can't be disregarded. With the contribution of this technique to the modern low radar cross-section systems, Lockheed Martin produced F-117 Stealth Fighter airplane.

2.4 Theory of Line Integrals

The diffraction phenomenon is based on the radiation and interference properties of waves. Early interpretation about diffraction process is observed by Newton's explanation. According to Newton, light consists of particles. Hence, diffraction is a natural result of the compelling effect of discontinuities on the particles. However, Young proved the wave nature of the light with his well known double slit experiment in 1802 [55]. Young first proposed the physical meaning of the scattered fields from a knife edge by the superposition of the incident and edge diffracted fields. It is important to note that scattering integral consists of the surface integral. Hence, for obtaining the edge diffracted fields, total surface integral has to be reduced to line integral. The similar procedure was applied by Maggi and Rubinowicz [33-34]. Maggi and Rubinowicz showed independently that Kirchhoff's integral can be decomposed as the sum of two terms. The first one represents the undisturbed wave which is directly propagates through an aperture and the second one represents the diffracted wave. In the introduction part, similar studies of authors about the reduction process were mentioned. In this part, we will concentrate on the reduction of the Kirchhoff's surface integral to a line integral in order to directly

obtain the edge diffracted field. The investigation of the diffracted fields from a half-plane will be illustrated.

The scattering surface is given in Fig. 4. The half-plane is lying on the surface $\{x \in [0,\infty), y = 0, z \in (-\infty,\infty)\}$. The total field is equal to zero according to the Dirichlet (soft) boundary condition.
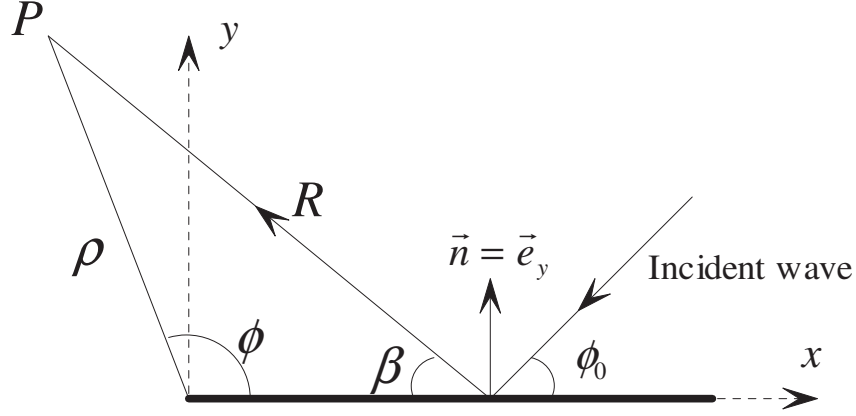
Figure 4 The geometry of the soft half-plane

The Kirchhoff's surface integral is given as

$$u(P) = \frac{1}{4\pi} \iint_S [u\nabla G - G\nabla u] \cdot \vec{n} dS \tag{2.8}$$

where u is the total field, G is the Green's function and $\vec{n}$ is the unit normal vector of the surface, respectively. The Dirichlet boundary condition is written as

$$u|_S = 0. \tag{2.9}$$

The surface is illuminated with the plane wave of

$$u_i = u_0 e^{jk(x\cos\phi_0 + y\sin\phi_0)} \tag{2.10}$$

where u_0 is the any component of the electric or magnetic field. After application of Eq. (2.9) to Eq. (2.8), according to PO the expression is

$$u(P) = \frac{1}{4\pi} \iint_{S'} G \frac{\partial u}{\partial n} dS' \tag{2.11}$$

where $\partial u / \partial n$ is equal to $\partial u / \partial y$. Total field is written as

$$u = 2u_i \tag{2.12}$$

Hence Eq. (2.11) is written as

14

$$u(P) = -\frac{jk \sin \phi_0}{2\pi} \int\limits_{x'=0}^{\infty} \int\limits_{z'=-\infty}^{\infty} e^{jkx' \sin \phi_0} \frac{e^{-jkR}}{R} dx' dz' \qquad (2.13)$$

where R is the ray path and equal to $\left[(x-x')^2 + y^2 + (z-z')^2 \right]^{\frac{1}{2}}$. The x' part can be reduced asymptotically by the well-known edge point technique [11]. The edge point technique is written as

$$\int\limits_{a}^{\infty} f(x)e^{-jkg(x)}dx \approx \frac{1}{jk} \frac{f(a)}{g'(a)} e^{-jkg(a)} . \qquad (2.14)$$

The phase function of Eq. (2.13) is written as

$$g(x') = x' \cos \phi_0 - R . \qquad (2.15)$$

The first derivative of the phase function is obtained as

$$\frac{dg}{dx'} = \cos \phi_0 + \frac{x - x'}{R} \qquad (2.16)$$

where $x-x'/R$ is equal to $-\cos \alpha$ from Fig. 5.
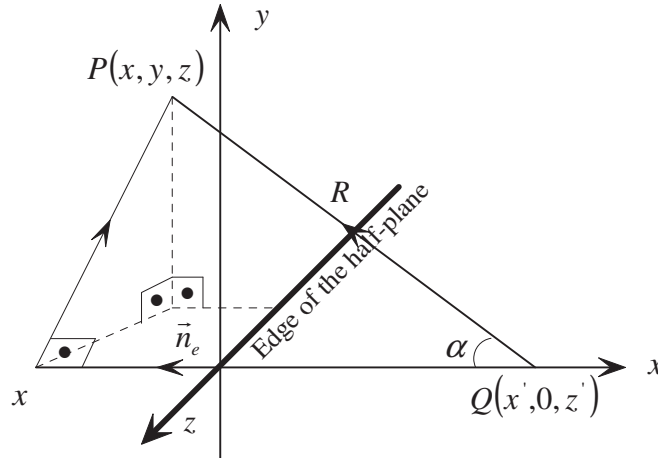

Figure 5 The angles of the scattered field

The phase function takes the form as

$$g(0) = -R_e \qquad (2.17)$$

at the edge of the scatterer where R_e is the ray path from edge to observation point P and equal to $\left[\rho^2 + (z-z')^2 \right]^{\frac{1}{2}}$. The first derivative of phase function of Eq. (2.15) is given by

$$g'(0) = \cos \phi_0 - \cos \alpha_e \qquad (2.18)$$

keep in mind that α is equal to α_e at the edge. The amplitude function is obtained as

$$f(0) = \frac{1}{R_e}$$ (2.19)

at the edge. After the application of the edge point technique, Eq. (2.13) is rewritten as

$$u_d(P) = -\frac{1}{2\pi} \int_{z'=-\infty}^{\infty} \frac{\sin\phi_0}{\cos\phi_0 - \cos\alpha_e} \frac{e^{-jkR_e}}{R_e} dz'$$ (2.20)

and reduced form of the surface integral is obtained. The Fig. 6 shows the angles of generalization process.
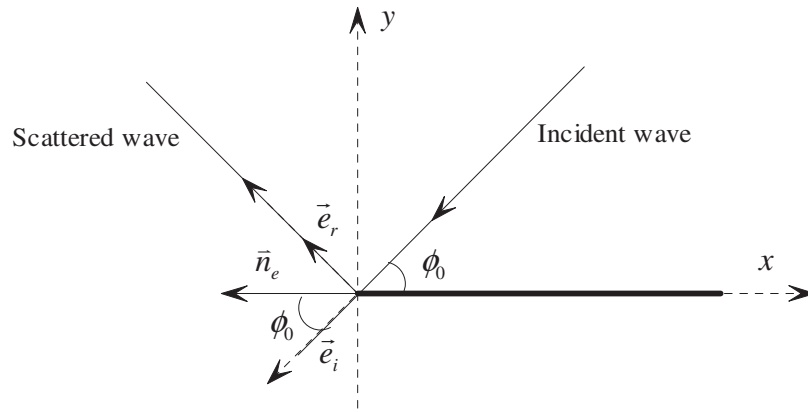
Figure 6 The angles of generalization process

The angles can be represented in terms of the unit vectors. They can be written as

$$\sin\phi_0 = \left\| \vec{n}_e \times \vec{n}_i \right\|,$$ (2.21)

$$\cos\phi_0 = \vec{n}_e \times \vec{e}_i$$ (2.22)

and

$$\cos\alpha_e = \vec{n}_e \times \vec{e}_r$$ (2.23)

respectively.

Hence, the generalized edge diffraction integral is derived as

$$u_d(P) = -\frac{1}{2\pi} \int_C \frac{\left\| \vec{n}_e \times \vec{e}_i \right\|}{\vec{n}_e \cdot (\vec{e}_i - \vec{e}_r)} \frac{e^{-jkR_e}}{R_e} dl$$ (2.24)

for an arbitrary soft surface.

CHAPTER 3

DIFFRACTION BY CYLINDERS

3.1 Diffraction by a Perfectly Electric Conducting Cylinder

This part is based on the M.Sc. thesis and the papers by Başdemir H. D. [30-31].

In this section, the field generated by the uniform component of the surface current, which is called the PO part, is calculated. This part is used for the examination of the radiated field by non-uniform component of the surface current. PTD is applied as the difference between the exact and PO fields. Hence, the effect of the non-uniform component to the scattered field is observed. Perfectly electric conducting (PEC) surface is taken into account. PEC means that total electric field on the tangential plane is equal to zero. This determination comes from the acoustic. Due to the definition of acoustic, this surface is called hard surface. The geometry of the problem is given in Fig. 7.
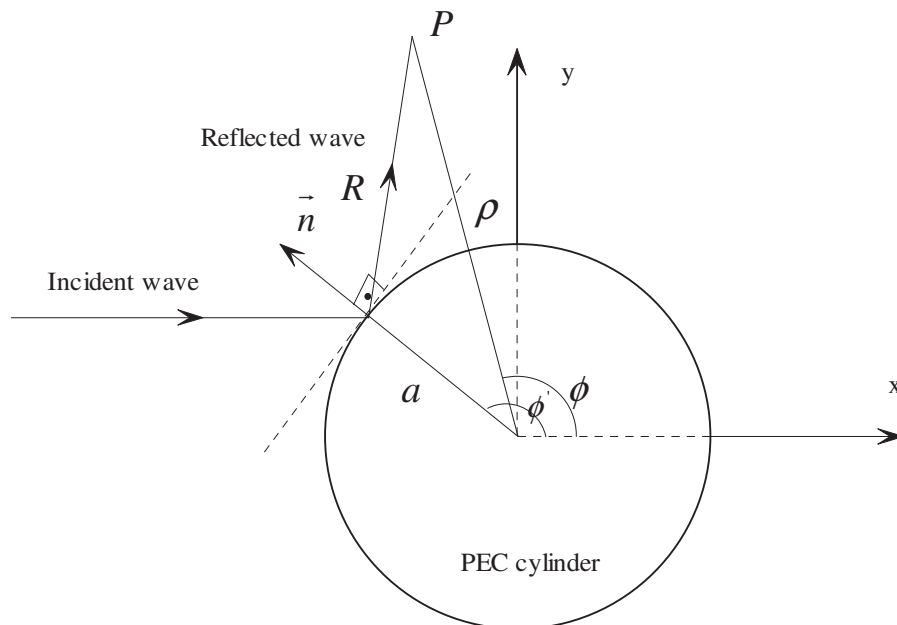

Figure 7 The Geometry of the PEC cylinder

The PEC cylinder is illuminated by the plane wave of

$$\vec{E}_i = \vec{e}_z E_0 e^{-jkx} \tag{3.1}$$

where E_0 is the complex amplitude factor and the incident wave is z polarized. The induced electric surface current can be defined as

$$\vec{J}_{PO} = 2\vec{n} \times \vec{H}_i \big|_s \tag{3.2}$$

where $\vec{n}$ is the unit normal vector and equal to $\vec{e}_\rho$. Incident magnetic field component is obtained from the Maxwell-Faraday equations as

$$\vec{H}_i = \frac{E_0 k}{\omega\mu_0} \left(-\vec{e}_\rho \sin\phi e^{-jk\rho\cos\phi} + \vec{e}_\phi \cos\phi e^{-jk\rho\cos\phi} \right) \tag{3.3}$$

Using the Eq. (3.3) under the surface condition,

$$\vec{J}_{PO} = 2\vec{n} \times \vec{H}_i \big|_{\rho=a} = \vec{e}_z \frac{2E_0 k}{\omega\mu_0} \cos\phi' e^{-jka\cos\phi'} \tag{3.4}$$

PO current is written. For simplification of the current, speed of light $c = \dfrac{1}{\sqrt{\varepsilon_0\mu_0}}$ and wave number $k = \dfrac{\omega}{c}$ are used. Reconstruction of the current is then given by

$$\vec{J}_{PO} = \vec{e}_z \frac{2E_0}{Z_0} \cos\phi' e^{-jka\cos\phi'} \tag{3.5}$$

where Z_0 is the impedance of the vacuum. PO scattering integral can be constructed by using the magnetic vector potential. Magnetic vector potential is written as

$$\vec{A} = \frac{\mu_0}{4\pi} \iint_{S'} \vec{J}_{PO} \frac{e^{-jkR}}{R} dS' \tag{3.6}$$

for the PO current. PO current is inserted into Eq. (3.10) and the integral of magnetic vector potential is obtained as

$$\vec{A} = \vec{e}_z \frac{\mu_0}{2\pi} \int_{z'=-\infty}^{\infty} \int_{\phi'=\frac{\pi}{2}}^{\frac{3\pi}{2}} \frac{E_0}{Z_0} \cos\phi' e^{-jka\cos\phi'} \frac{e^{-jkR}}{R} a d\phi' dz' \tag{3.7}$$

where a is the radius of the cylinder. The z' part of the integral can be evaluated as

$$\int_C e^{-jk\cosh\alpha} d\alpha = \frac{\pi}{j} H_0^{(2)}(kR) \tag{3.8}$$

As a result, Eq. (3.7) takes the form of

$$\vec{A} = \vec{e}_z \frac{\mu_0 E_0 a}{2 Z_0 j} \int_{\phi'=\frac{\pi}{2}}^{\frac{3\pi}{2}} \cos\phi' e^{-jka\cos\phi'} H_0^{(2)}(kR_1) d\phi' \tag{3.9}$$

where R_1 is the ray path and equal to $\sqrt{\rho^2 + a^2 - 2\rho a \cos(\phi - \phi')}$. The expression of the uniform scattered electric field is obtained from

$$\vec{E}_s \cong -j\omega\vec{A} \tag{3.10}$$

where this notation is valid for the far field which is $k\rho \gg 1$. Hence, uniform scattered electric field expression is obtained as

$$\vec{E}_s^{PO} = \vec{e}_z \frac{-\omega\mu_0 E_0 a}{2 Z_0} \int_{\phi'=\frac{\pi}{2}}^{\frac{3\pi}{2}} \cos\phi' e^{-jka\cos\phi'} H_0^{(2)}(kR_1) d\phi' \tag{3.11}$$

Total exact scattered field from the cylinder can be written as

$$\vec{E}_s^{total} = \vec{e}_z E_0 \sum_{n=-\infty}^{\infty} j^{-n} a_n H_n^{(2)}(k\rho) e^{jn\phi} \tag{3.12}$$

and

$$a_n = \frac{-J_n(ka)}{H_n^{(2)}(ka)} \tag{3.13}$$

for magnetic polarization case from the Ref. [56]. The terms J_n, H_n are the zeroth order and the third order Bessel functions respectively. Specifically, the third order Bessel function is called Hankel function and a is radius of the cylinder. According to PTD method, the contribution of non-uniform part is obtained as

$$\vec{E}_s^{NU} = \vec{E}_s^{total} - \vec{E}_s^{PO} \tag{3.14}$$

Using Eq. (3.11) non-uniform scattered electric field is written as

$$\vec{E}_s^{NU} = \vec{e}_z E_0 \sum_{n=-\infty}^{\infty} j^{-n} a_n H_n^{(2)}(k\rho) + \vec{e}_z \frac{\omega\mu_0 E_0 a}{2 Z_0} \int_{\phi'=\frac{\pi}{2}}^{\frac{3\pi}{2}} \cos\phi' e^{-jka\cos\phi'} H_0^{(2)}(kR_1) d\phi' \tag{3.15}$$

which is the exact scattered non-uniform field. Another way to find the non-uniform field is evaluating non-uniform current over the surface of the cylinder so that non-uniform current have to be written. Surface current on the cylinder is written as

$$\vec{J}_{exact}^{surface} = \vec{e}_z \frac{-2E_0}{\omega\mu\pi a} \sum_{n=-\infty}^{\infty} \frac{j^{-n} e^{jn\phi}}{H_n^{(2)}(ka)} \tag{3.16}$$

for PEC case from Ref. [56]. From Eq. (3.5) PO current is written as

$$\vec{J}_{PO} = \vec{e}_z \frac{2E_0}{Z_0} \cos\phi \, e^{-jka\cos\phi} \tag{3.17}$$

The non-uniform current is obtained as

$$\vec{J}_{NU} = \vec{J}_{exact}^{surface} - \vec{J}_{PO} \tag{3.18}$$

according to PTD [5]. Hence, non-uniform current takes the form of

$$\vec{J}_{NU} = \vec{e}_z \frac{-2E_0}{\omega\mu\pi a} \sum_{n=-\infty}^{\infty} \frac{j^{-n} e^{jn\phi}}{H_n^{(2)}(ka)} - \vec{e}_z \frac{2E_0}{Z_0} \cos\phi \, e^{-jka\cos\phi} \tag{3.19}$$

when Eq. (3.18) is used. When Eq. (3.6) is used, magnetic vector potential is constructed as

$$\vec{A}_{NU} = \vec{e}_z \frac{\mu_0}{2\pi} \int_{z'=-\infty}^{\infty} \int_{\phi'=0}^{2\pi} \left[\frac{-E_0}{\omega\mu\pi a} \sum_{n=-\infty}^{\infty} \frac{j^{-n} e^{jn\phi'}}{H_n^{(2)}(ka)} - \frac{E_0}{Z_0} \cos\phi' \, e^{-jka\cos\phi'} \right] \frac{e^{-jkR}}{R} a \, d\phi' dz' \tag{3.20}$$

for non-uniform scattered field. The z' part of the integral is evaluated from the Eq. (3.8) so non-uniform scattered field takes the form of

$$\vec{A}_{NU} = \vec{e}_z \frac{-\mu_0 E_0}{2j\omega\mu\pi} \sum_{n=-\infty}^{\infty} \frac{j^{-n}}{H_n^{(2)}(ka)} \int_{\phi'=0}^{2\pi} e^{jn\phi'} H_0^{(2)}(kR_1) d\phi'$$

$$- \vec{e}_z \frac{\mu_0 a E_0}{2jZ_0} \int_{\phi'=0}^{2\pi} \cos\phi' H_0^{(2)}(kR_1) d\phi' \tag{3.21}$$

where R_1 is the ray path and equal to $\sqrt{\rho^2 + a^2 - 2\rho a \cos(\phi - \phi')}$. Evaluation of this integral directly gives exact scattered non-uniform electric field. The expression of PO should be translated into the series form for obtaining the non-uniform part. After this transformation, by using the exact known scattered total field, non-uniform exact solution can be obtained in the series form.

3.2 Diffraction by an Impedance Cylinder

The geometry of the problem is given in the Fig. 8. The radius of the cylinder is a, $\pi - \phi'$ is the incident angle and $\vec{n}$ is the unit normal vector.
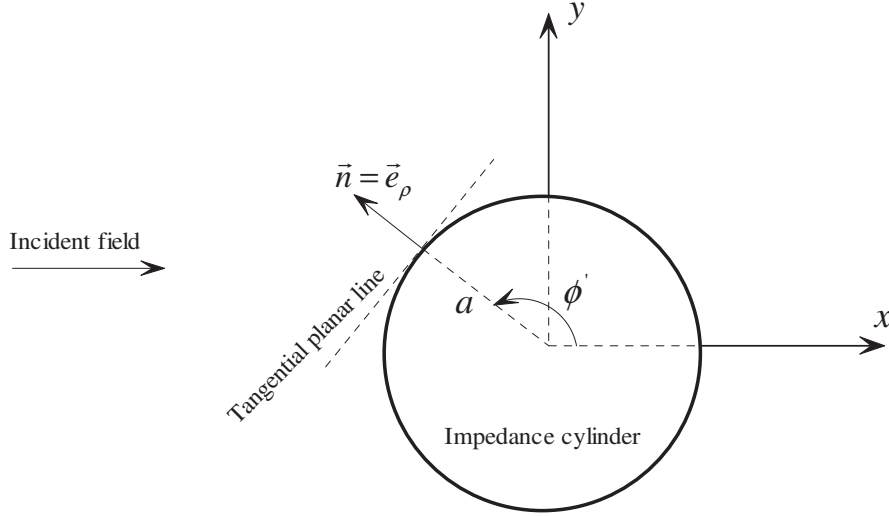
Figure 8 The impedance cylinder geometry

The geometry is illuminated by the transverse magnetic polarized (TM) plane wave of

$$\vec{E}_i = \vec{e}_z E_0 e^{-jk\rho\cos\phi} \tag{3.22}$$

where E_0 is the complex amplitude factor. PO currents can be described on the tangential planar line as

$$\vec{J}_e^{PO} = \vec{n} \times \vec{H}_t \big|_s \tag{3.23}$$

and

$$\vec{J}_m^{PO} = -\vec{n} \times \vec{E}_t \big|_s \tag{3.24}$$

where $\vec{E}_t$, $\vec{H}_t$ are the total electric and magnetic fields respectively and $\vec{n}$ is the unit normal vector of the tangential planar line of the surface and is equal to $\vec{e}_\rho$ in this case. The total GO field is the combination of the incident and reflected fields. The total GO field can be written as

$$\vec{E}_t = \vec{E}_i + \Gamma \vec{E}_r \qquad (3.25)$$

where $\Gamma(\phi', \theta) = \dfrac{\sin \phi' - \sin \theta}{\sin \phi' + \sin \theta}$ is the reflection coefficient and also known as the

Fresnel coefficient [57]. According to the PO approximation, reflected field has the same structure with respect to the incident field. In light of this definition, total GO field is written as

$$\vec{E}_t\big|_s = \left(\vec{E}_i + \Gamma \vec{E}_i\right)\big|_s = \vec{E}_i (1 + \Gamma)\big|_s \qquad (3.26)$$

from the Ref. [57]. PO magnetic current is constructed as

$$\vec{J}_m^{PO}\big|_s = \vec{e}_\phi E_0 e^{-jka\cos\phi'} (1 + \Gamma) \qquad (3.27)$$

taking into account the Eq. (3.24). Total scattered PO electric field is given as

$$\vec{E}_{PO} \cong -j\omega \vec{A} - \frac{1}{\varepsilon_0} \nabla \times \vec{F} \qquad (3.28)$$

where $\vec{A}$ is the magnetic vector potential and $\vec{F}$ is the electric vector potential. Electric vector potential can be found

$$\vec{F} = \frac{\varepsilon_0}{4\pi} \iint_{S'} \vec{J}_m^{PO} \frac{e^{-jkR}}{R} dS' \qquad (3.29)$$

after the evaluation of this integral expression. Before the evaluation process, the result of the rotation operation has to be found for total PO scattered field. Hence, Eq. (3.29) is rewritten as

$$\frac{1}{\varepsilon_0} \nabla \times \vec{F} = \nabla \times \left(\frac{1}{4\pi} \int_{\phi'=\frac{\pi}{2}}^{\frac{3\pi}{2}} \int_{z'=-\infty}^{\infty} \vec{e}_\phi E_0 e^{-jka\cos\phi'} (1 + \Gamma) \frac{e^{-jkR}}{R} a\, dz'\, d\phi' \right) \qquad (3.30)$$

according to Eq. (3.28) where a is the radius of the impedance cylinder, R is the ray path and equal to $\sqrt{\rho^2 + a^2 - 2\rho a \cos(\phi - \phi') + (z - z')^2}$. The z' part of Eq. (3.30) can be simplified as

$$\int_c e^{-jkR_1 \cosh\alpha} d\alpha = \frac{\pi}{j} H_0^{(2)}(kR_1) \qquad (3.31)$$

with using the variable change $z - z' = R_1 \sinh\alpha$ where R_1 is equal to $\sqrt{\rho^2 + a^2 - 2\rho a \cos(\phi - \phi')}$. Hankel function's Debby asymptotic form is given as

22

$$H_0^{(2)}(kR_1) \approx \sqrt{\frac{2}{\pi}} e^{j\frac{\pi}{4}} \frac{e^{-jkR_1}}{\sqrt{kR_1}} \qquad (3.32)$$

The Eq. (3.30) is rewritten as

$$\frac{1}{\varepsilon_0} \nabla \times \vec{F} = \frac{aE_0 e^{-j\frac{\pi}{4}}}{2\sqrt{2\pi}} \int_{\phi'=\frac{\pi}{2}}^{\frac{3\pi}{2}} e^{-jka\cos\phi'} (1+\Gamma)\nabla \times \left(\vec{e}_\phi \frac{e^{-jkR_1}}{\sqrt{kR_1}} \right) d\phi' \qquad (3.33)$$

with respect to Eq. (3.31) and Eq. (3.32). The curl operation is given as

$$\nabla \times \left(\vec{e}_\phi \frac{e^{-jkR_1}}{\sqrt{kR_1}} \right) = \frac{1}{\rho} \begin{vmatrix} \vec{e}_\rho & \rho\vec{e}_\phi & \vec{e}_z \\ \dfrac{\partial}{\partial\rho} & \dfrac{\partial}{\partial\phi} & 0 \\ 0 & \rho\dfrac{e^{-jkR_1}}{\sqrt{kR_1}} & 0 \end{vmatrix} \qquad (3.34)$$

where the result can be found as

$$\nabla \times \left(\vec{e}_\phi \frac{e^{-jkR_1}}{\sqrt{kR_1}} \right) = \vec{e}_z \frac{1}{\rho} \left(\frac{\partial}{\partial\rho} \rho \frac{e^{-jkR_1}}{\sqrt{kR_1}} \right). \qquad (3.35)$$

Hence, curl operation in Eq. (3.34) is approximately equal to

$$\nabla \times \left(\vec{e}_\phi \frac{e^{-jkR_1}}{\sqrt{kR_1}} \right) \cong \frac{e^{-jkR_1}}{\sqrt{kR_1}} \left(1 - jk\frac{\partial R_1}{\partial\rho} \rho \right). \qquad (3.36)$$

where $\dfrac{\partial R_1}{\partial\rho}$ is equal to $\dfrac{\rho - a\cos(\phi - \phi')}{R_1}$. The result of curl operation is obtained as

$$\nabla \times \left(\vec{e}_\phi \frac{e^{-jkR_1}}{\sqrt{kR_1}} \right) = \frac{e^{-jkR_1}}{\sqrt{kR_1}} \left(\frac{1}{\rho} - \frac{jk(\rho - a\cos(\phi - \phi'))}{R_1} \right) \qquad (3.37)$$

where $\dfrac{1}{\rho}$ can be neglected because of $k \gg 1$. Hence the final expression of Eq. (3.33) is found as

$$\frac{1}{\varepsilon_0} \nabla \times \vec{F} = -\vec{e}_z \frac{aE_0 k e^{j\frac{\pi}{4}}}{2\sqrt{2\pi}} \int_{\phi'=\frac{\pi}{2}}^{\frac{3\pi}{2}} \left[\frac{\rho - a\cos(\phi - \phi')}{R_1} \right] (1+\Gamma)e^{-jka\cos\phi'} \frac{e^{-jkR_1}}{\sqrt{kR_1}} d\phi' \qquad (3.38)$$

PO electric current can be found from Eq. (3.23). Total magnetic field in Eq. (3.23) is found from the Maxwell's equations as

$$\vec{H}_t = -\frac{1}{j\omega\mu_0\rho} \begin{vmatrix} \vec{e}_\rho & \rho\vec{e}_\phi & \vec{e}_z \\ \dfrac{\partial}{\partial\rho} & \dfrac{\partial}{\partial\phi} & 0 \\ 0 & 0 & \left(\vec{E}_i + \Gamma\vec{E}_r\right) \end{vmatrix} \tag{3.39}$$

where total magnetic field is obtained as

$$\vec{H}_t = -\frac{1}{j\omega\mu_0\rho}\left(\vec{e}_\rho \frac{\partial E_{tz}}{\partial\phi} - \rho\vec{e}_\phi \frac{\partial E_{tz}}{\partial\rho}\right) \tag{3.40}$$

PO electric current which is given in Eq. (3.23) is obtained as

$$\vec{J}_e^{PO}\Big|_s = -\vec{e}_z \frac{E_0 \cos\phi'}{Z_0} e^{-jka\cos\phi'}\left(1-\Gamma\right) \tag{3.41}$$

where Z_0 is the impedance of the vacuum. Magnetic vector potential $\vec{A}$ can be written as

$$\vec{A} = \frac{\mu_0}{4\pi}\iint_S \vec{J}_e^{PO} \frac{e^{-jkR}}{R} dS \tag{3.42}$$

The integral is constructed as

$$\vec{A} = -\vec{e}_z \frac{\mu_0 a E_0 e^{-j\frac{\pi}{4}}}{2\sqrt{2\pi}Z_0} \int_{\phi'=\frac{\pi}{2}}^{\frac{3\pi}{2}} \cos\phi' e^{-jka\cos\phi'}\left(1-\Gamma\right)\frac{e^{-jkR_1}}{\sqrt{kR_1}} d\phi' \tag{3.43}$$

using with Eq. (3.41) and simplification of z' part as same as Eq. (3.30). The Eq. (3.43) is rearranged as

$$-j\omega\vec{A} = \vec{e}_z \frac{aE_0 k e^{j\frac{\pi}{4}}}{2\sqrt{2\pi}} \int_{\phi'=\frac{\pi}{2}}^{\frac{3\pi}{2}} \cos\phi' e^{-jka\cos\phi'}\left(1-\Gamma\right)\frac{e^{-jkR_1}}{\sqrt{kR_1}} d\phi' \tag{3.44}$$

according to Eq. (3.28). Hence, total scattered PO field can be found as

$$\vec{E}_{PO} \cong \vec{e}_z \frac{E_0 k a e^{j\frac{\pi}{4}}}{2\sqrt{2\pi}} \int_{\phi'=\frac{\pi}{2}}^{\frac{3\pi}{2}} \left[\cos\phi' + \frac{\rho - a\cos(\phi-\phi')}{R_1}\right]$$

$$\times\left(1-\Gamma\right)e^{-jka\cos(\phi-\phi')}\frac{e^{-jkR_1}}{\sqrt{kR_1}} d\phi \tag{3.45}$$

with the combination of Eq. (3.38) and Eq. (3.42) according to Eq. (3.28). Total scattered or the exact scattered field from an impedance cylinder can be found under the considerations of the impedance boundary conditions. Impedance boundary condition is given as

$$\vec{n} \times \vec{n} \times \vec{E}_t \Big|_s = -Z\vec{n} \times \vec{H}_t \Big|_s \tag{3.46}$$

where $\vec{n}$ is unit normal vector Z, $\vec{E}_t$, $\vec{H}_t$ are impedance of scatterer, total electric and magnetic fields respectively. Total electric field can be obtained after the wave transform is applied to the incident electric field. The wave transform is defined as

$$e^{-jkx} = e^{-jka\cos\phi'} = \sum_{n=-\infty}^{\infty} j^{-n} J_n(ka) e^{jn\phi'} \tag{3.47}$$

from Ref. [56]. Total electric field is defined as

$$\vec{E}_t = \vec{E}_i + \vec{E}_s \tag{3.48}$$

where $\vec{E}_s$ is the scattered electric field from the cylinder and it is written as

$$\vec{E}_s = \vec{e}_z E_0 \sum_{n=-\infty}^{\infty} j^{-n} a_n H_n^{(2)}(k\rho) e^{jn\phi} \tag{3.49}$$

from Ref. [56]. In this case, total electric field's expression is obtained as

$$\vec{E}_t = \vec{e}_z E_0 \sum_{n=-\infty}^{\infty} j^{-n} \left[J_n(k\rho) + a_n H_n^{(2)}(k\rho) \right] e^{jn\phi} \tag{3.50}$$

in terms of the series solution. Total magnetic field is found as

$$\vec{H}_t = -\frac{1}{j\omega\mu_0\rho} \left(\vec{e}_\rho \frac{\partial E_z}{\partial \phi} - \rho\vec{e}_\phi \frac{\partial E_z}{\partial \rho} \right) \tag{3.51}$$

after application of the Maxwell's equations to Eq. (3.50). According to the impedance boundary condition, the term a_n can be obtained from

$$-\vec{e}_z E_0 \sum_{n=-\infty}^{\infty} j^{-n} \left[J_n(ka) + a_n H_n^{(2)}(ka) \right] e^{jn\phi} \Bigg|_{\rho=a}$$

$$= -Z\vec{e}_z \frac{1}{j\omega\mu_0} \left\{ E_0 \sum_{n=-\infty}^{\infty} j^{-n} \left[J_n^{'}(ka) + a_n H_n^{(2)'}(ka) \right] e^{jn\phi} \right\} \Bigg|_{\rho=a} \tag{3.52}$$

Hence, a_n is found as

$$a_n = \frac{jkZ_0 J_n(ka) - ZJ_n^{'}(ka)}{ZH_n^{(2)'}(ka) - jkZ_0 H_n^{(2)}(ka)} \tag{3.53}$$

Under the consideration of the impedance boundary condition, total scattered electric field is found as

$$\vec{E}_t = \vec{e}_z E_0 \sum_{n=-\infty}^{\infty} j^{-n} \left[J_n(k\rho) + a_n H_n^{(2)}(k\rho) \right] e^{jn\phi'} \tag{3.54}$$

where

$$a_n = \frac{jk\sin\theta J_n(ka) - J_n'(ka)}{H_n^{(2)'}(ka) - jk\sin\theta H_n^{(2)}(ka)}. \tag{3.55}$$

The term $\sin\theta$ is the impedance factor and equal to $\frac{Z_0}{Z}$ where Z_0 is impedance of vacuum and Z is impedance of scatterer. According to PTD method, total scattered electric field can be described as

$$\vec{E}_t = \vec{E}_{PO} + \vec{E}_{NU} \tag{3.56}$$

with the combination of PO and the contribution of non-uniform fields. The contribution of the non-uniform part to the scattered electric field can be found

$$\vec{E}_{NU} = \vec{E}_t - \vec{E}_{PO} \tag{3.57}$$

Non-uniform obtained as

$$\vec{E}_{NU} = \vec{e}_z E_0 \left\{ \sum_{n=-\infty}^{\infty} j^{-n} \left[J_n(k\rho) + a_n H_n^{(2)}(k\rho) \right] e^{jn\phi'} - \right.$$

$$\left. \frac{kae^{j\frac{\pi}{4}}}{2\sqrt{2\pi}} \int_{\phi'=\frac{\pi}{2}}^{\frac{3\pi}{2}} \left(\cos\phi' + \frac{\rho - a\cos(\phi-\phi')}{R} \right)(1+\Gamma)e^{-jka\cos(\phi-\phi')} \frac{e^{-jkR_1}}{\sqrt{kR_1}} d\phi' \right\} \tag{3.58}$$

with respect to the PTD method. According to PTD, total currents can be described as

$$\vec{J}_{mt} = \vec{J}_m^{PO} + \vec{J}_m^f \tag{3.59}$$

and

$$\vec{J}_{et} = \vec{J}_e^{PO} + \vec{J}_e^f \tag{3.60}$$

where $\vec{J}_{mt}$ is the total magnetic current, $\vec{J}_{et}$ is the total electric current and $\vec{J}_m^f$, $\vec{J}_e^f$ are the magnetic and electric fringe currents. Total currents are found from the Eq. (3.23), Eq. (3.24) and Eq. (3.46). The relation between total electric and magnetic currents is written as

$$\vec{J}_{et} = \frac{1}{Z}\vec{n} \times \vec{J}_{mt} \tag{3.61}$$

under considerations of Eq. (3.23), Eq. (3.24) and Eq. (3.46). Total magnetic current is written as

$$\vec{J}_{mt}\Big|_s = \vec{e}_\phi E_0 \sum_{n=-\infty}^{\infty} j^{-n} \left[J_n(ka) + a_n H_n^{(2)}(ka) \right] e^{jn\phi'} \tag{3.62}$$

26

where a_n was described before. Magnetic fringe current can be given by

$$\vec{J}_m^f = \vec{J}_{mt} - \vec{J}_m^{PO} \tag{3.63}$$

for definition of PTD. Magnetic fringe current is written as

$$\vec{J}_m^f = \vec{e}_\phi E_0 \left\{ \sum_{n=-\infty}^{\infty} j^{-n} \left[J_n(ka) + a_n H_n^{(2)}(ka) \right] e^{jn\phi'} - e^{-jka\cos\phi'} (1+\Gamma) \right\} \tag{3.64}$$

Same procedure is valid for electrical fringe current. Hence, electrical fringe current can be found

$$\vec{J}_e^f = \vec{J}_{et} - \vec{J}_e^{PO} \tag{3.65}$$

from definition of PTD. Total electric field is given by

$$\vec{J}_{et}\Big|_s = \vec{e}_z \frac{E_0}{Z} \sum_{n=-\infty}^{\infty} j^{-n} \left[J'_n(ka) + a_n H_n^{(2)'}(ka) \right] e^{jn\phi'} \tag{3.66}$$

from the Eq. (3.58). Electrical fringe current is obtained as

$$\vec{J}_e^f = \vec{e}_z E_0 \left\{ \frac{1}{Z} \sum_{n=-\infty}^{\infty} j^{-n} \left[J'_n(ka) + a_n H_n^{(2)'}(ka) \right] + \frac{1}{Z_0} \cos\phi' e^{-jka\cos\phi'} (1-\Gamma) \right\}. \tag{3.67}$$

3.3 Numerical Results

In this analysis part, numerical results for the nonuniform currents and the scattered fields will be investigated. In order to investigate the far field, the observation point is taken to a comprehensible distance from the scatterer. The distance between the source points to the observation point will be taken as 10λ, where λ is the wavelength. High frequency asymptotic techniques require that the size of the scatterer should be higher than the wave length of incident wave. Radius of the cylinder (a) will be taken as 5λ for the consistence of high frequencey condition. Impedance factor $\sin\theta$ will be taken as 4.
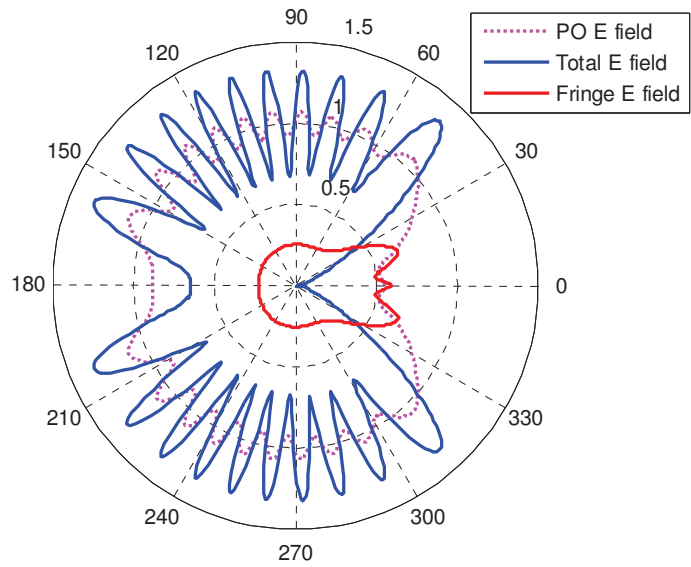
Figure 9 Scattered electrical fields from impedance cylinder

Figure 9 shows the total scattered fields. PO scattered field includes the diffracted fields and reflected fields. Amplitude variations approach to zero near 0° because of the wrong diffracted fields and the deficiency of the shadow part. Diffracted fringe field takes its maximum value near 0° and compensates these deficiencies of the PO scattered field. Total scattered field includes both reflected and diffracted fields. As can be seen in the Fig. 9 the amplitude of the total scattered field consists of the interference of the PO and fringe fields.
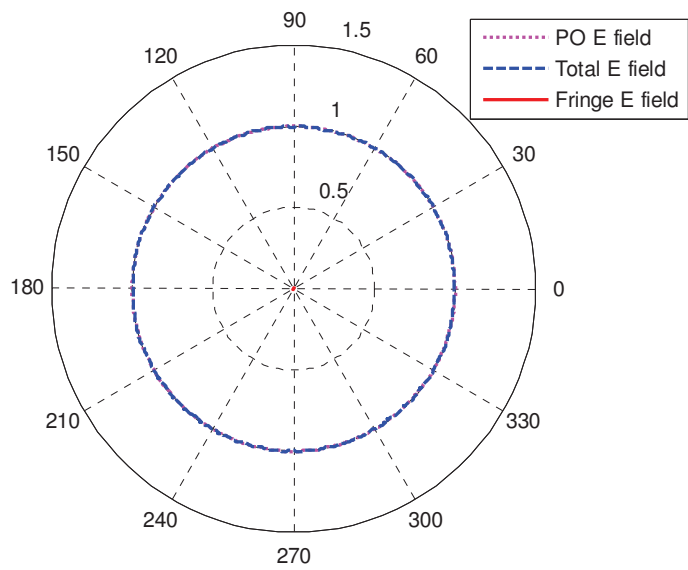
Figure 10 Scattered electrical fields from impedance cylinder for smaller radius

Figure 10 shows the scattered electric fields from impedance cylinder for the smaller radius of cylinder. As expected, cylinder acts as a line source thus electrical fields scattered by the cylinder equaly radiate to all directions. Hence, high frequency condition is not provided so cylinder acts as a line source not a scatterer.

Figure 11 Electrical currents flowing on impedance cylinder

Figure 11 shows the electrical currents which are induced by the incident field. In Fig. 11, current patterns become dominant on the reflection region. PO current takes maximum amplitude value between 120˚ and 240˚. PO currents amplitude values lead to zero value at 0˚. Because of the exclusion of the shadow part of the scatterer by the PO, there is not any amplitude values for the currents. Fringe current consists one main and two minor lobes and its maximum directivity occurs at the 180˚. The total electrical currents amplitude variation distrubutes equally at the reflection regions. Fringe current compensates the deficiency of PO in the shadow region and it can be analyzed especially in the minor lobes of fringe current in Fig. 11.
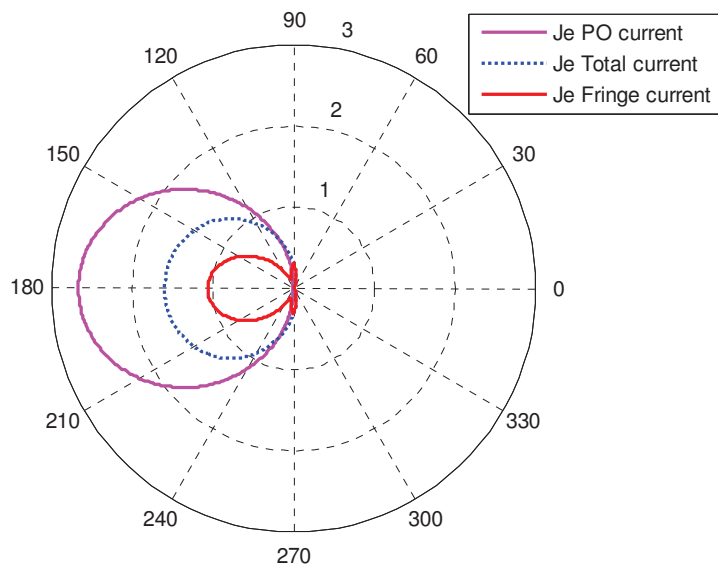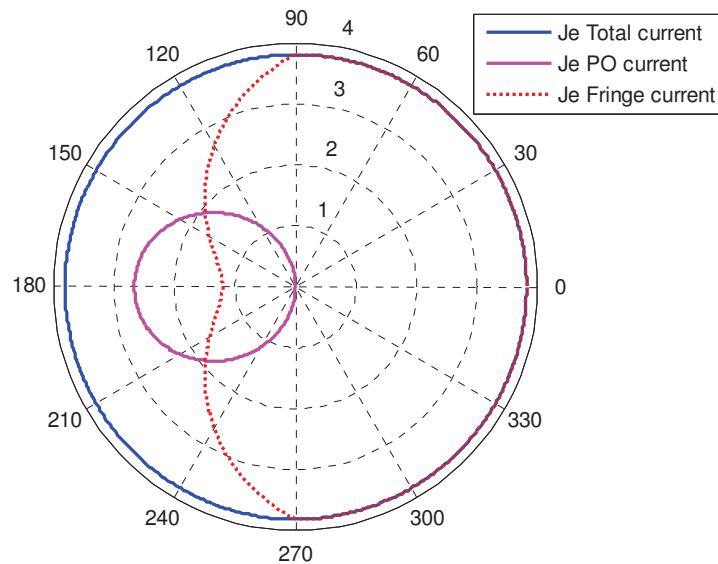

Figure 12 Electrical currents flowing on impedance cylinder for smaller radius

Figure 12 shows the electrical current distrubition over the impedance cylinder. In this case radius of cylinder is taken as smaller than one in Fig. 11. In the shadow region the distribution of the fringe and total current are the same. PO current distributes over the illumunated region. Also cylinder acts as line source in this figure and distrubition of total current is equal for all the observation directions.
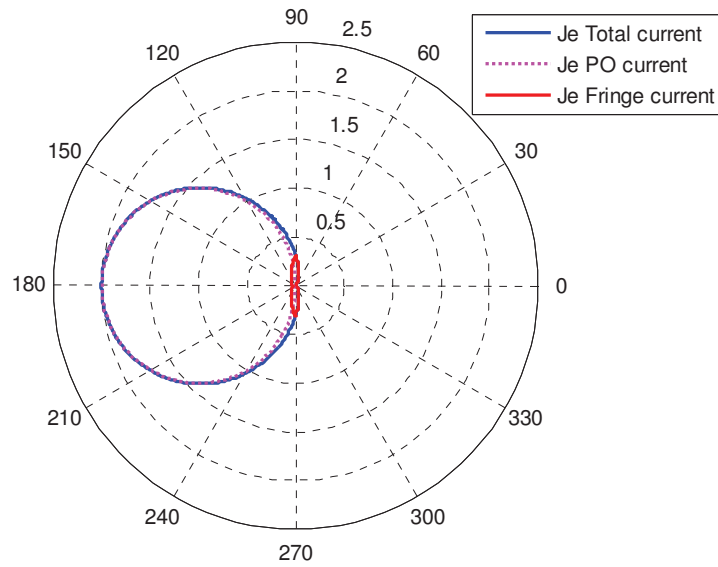
Figure 13 Electrical currents flowing on impedance cylinder for $\sin\theta \to \infty$

In Fig. 13 the behaviour of the surface is similar with the perfecly electric conducting surface. This behaviour is related with the value of $\sin\theta$ term, which is used in the reflection coefficient. When this term goes to infinity surface acts as a conducting surface. Hence the effect of the surface impedance is dependent on this term. There was no need to plot the magnetic currents for this case because of the boundary conditions of conducting surface predict zero magnetic current in the surface. The detailed explanations for the conducting case will be examined in the subsequent figures.

Figure 14 Magnetic currents flowing on impedance cylinder

Figure 14 shows the magnetic currents, which are induced by the incident field. In Fig. 14, current patterns become dominant on the reflection region like the Fig. 11. Fringe current has one main and two side lobes in Fig. 14. Main lobe takes its maximum amplitude values at 180° and the side lobes a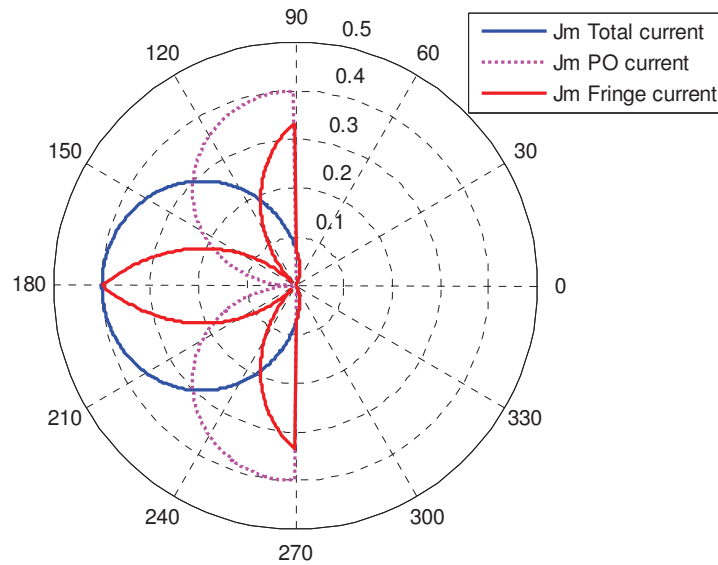mplitude values decrease towards to the shadow regions. Fringe currents compensate the deficiency of the PO currents in the shadow regions. The effect of the impedance is observed in both Fig. 11 and Fig. 14. Impedance surface absorbed a part of the incoming energy and decreased the amplitudes of the currents. Although the normalized results were plotted, due to effects of the impedance surface, amplitudes take smaller values.

In Fig. 15 radius of the cylinder is taken smaller than the one in Fig. 14. Hence, the total current distrubution is observed in all directions, PO current disribution is same with the previous case and fringe current distribution is the same like total current distribution in the shadow region. In the illuminated region fringe current amplitude takes its maximum values at 180° and decreases when the angles goes to boundary of illuminated regions. Also in this case due to the smaller radius cylinder reduces to a line source.
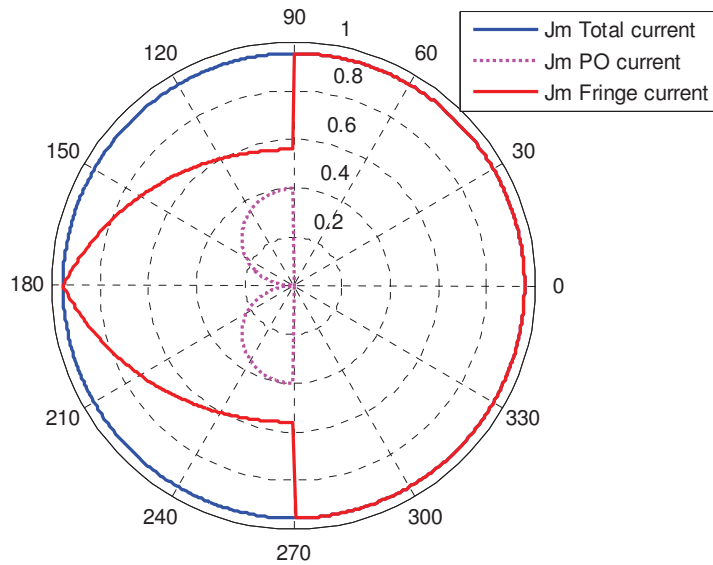
Figure 15 Magnetic currents flowing on impedance cylinder for small radius

For the PEC cylinder, the distance between the observation point and the origin will be taken as 5λ, which is constant for all plots, where λ is the wavelength. Radius of the cylinder (a) will be taken as 2λ in Fig. 16 and Fig. 17. Figure 16 shows the currents on the cylinder. The amplitudes of exact and uniform currents are between 120˚ and 240˚.Maximum amplitude is obtained at 180˚. Non-uniform current is the difference between the total current and the PO current. As it can be seen in the Fig. 16, the amplitude differences occur in the region bordered by the red line. Deficient current amplitude between the PO current and the exact current is accomplished by the non-uniform current amplitude.
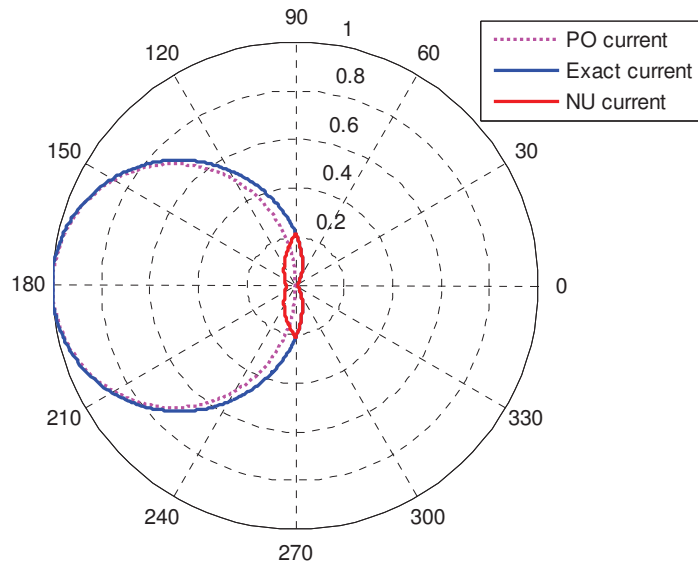
Figure 16 Electrical currents flowing on the PEC cylinder

Figure 17 shows the scattered fields. Non-uniform scattered field takes the finite values at the first and fourth regions. PO radiation exists only at the lit region, which is bounded by angles 90° and 270° and the scattered fields from the shadow part of the obstacle are excluded. As expected, the distribution of PO scattered fields amplitude is uniform between the 90° and 270° and exists in the shadow region. The exact total scattered electric fields amplitude is observed in all directions of observation. Radiation especially concentrates at the shadow region for PEC case. At 0° the total scattered electric fields amplitude takes maximum value. In accordance with the theory, non-uniform field distribution is observed in the shadow part of the scatterer. Like exact total field, non-uniform component of the scattered field takes maximum amplitude values at 0°. No amplitude variation is observed for non-uniform field in the lit region of the cylinder. The absent part of the exact fields in the shadow region is caused by the non-uniform scattered field.
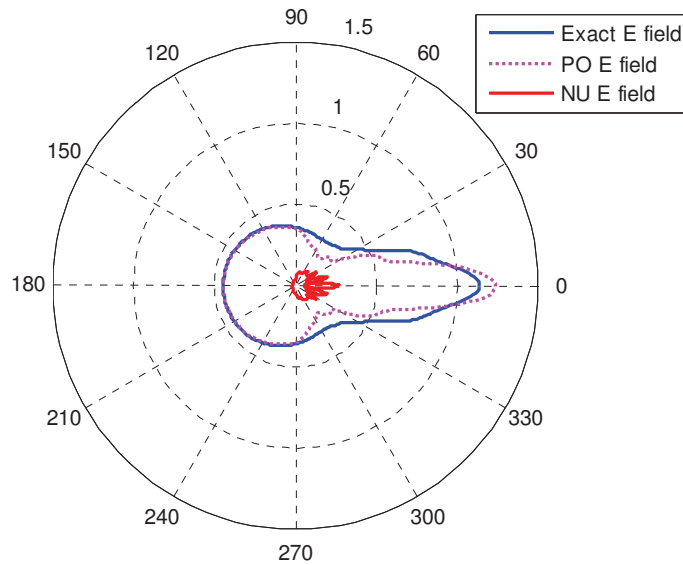
Figure 17 Scattered electric fields from PEC cylinder

Figure 18 shows the current distribution of for the smaller radius of PEC cylinder. PO current distribution does not change in this situation but the total current distributes uniformly for all directions of observation. Non-uniform current is obtained by subtracting the PO current from the total current. It can be seen from Fig. 18 that the effect of the PO current is rather small, as expected since the non-uniform current distribution is nearly the same like total current. A small difference between the non-uniform and total current is observed in the illuminated region because of the PO current's effect.

In Fig. 19 scattered electric fields are observed for the smaller radius of conducting cylinder. Total electric field amplitude distribution and non-uniform electric field distribution are almost the same. PO electric field amplitude is smaller than others. Also in this situation cylinder acts as a line source, not a scatterer, thus field distribution is observed in all directions of observation.

As a result, it can be observed that the radius of cylinder is directly related to the field or current distribution. Since the high frequency condition is not achieved in the smaller radius of the cylinder, cylinder acts as a line source. Hence, in this case high frequency methods are not preferred.
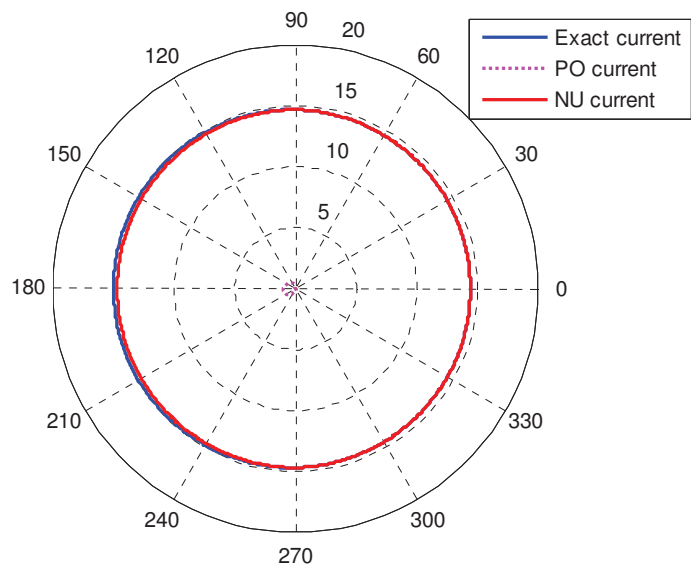
Figure 18 Electrical currents flowing on the PEC cylinder for smaller radius
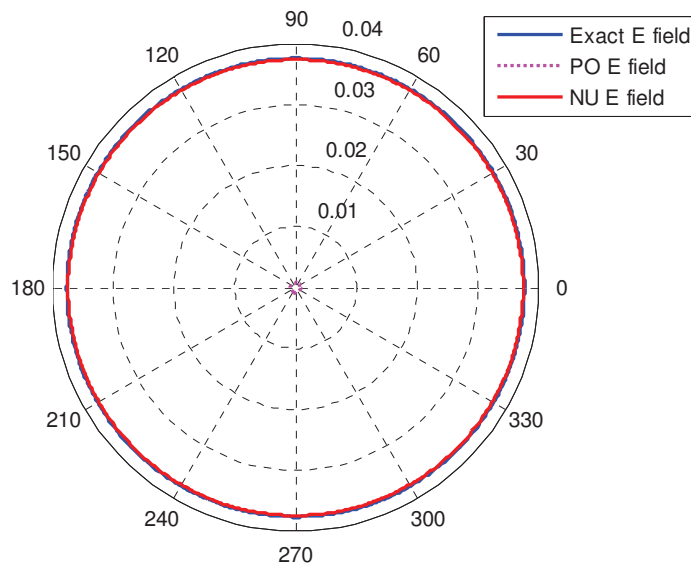
Figure 19 Scattered electric fields from PEC cylinder for smaller radius

CHAPTER 4

DIFFRACTION by PERFECTLY CONDUCTING EDGES

4.1 Perfectly Electric Conducting Half-Plane

In this part, general line integral representation of the fringe field expressions for PEC edges will be derived. The generalization process will start with the derivation of PO part for PEC edges. After that, fringe field expression will be obtained by using the exact diffracted field. Lastly, obtained expression will be transformed into general line integral representation with the aid of the unit vectors.

The geometry of the problem for PO diffracted field is given in Fig. 14. The half-plane is lying on the surface $\{x \in [0,\infty), y = 0, z \in (-\infty, \infty)\}$.
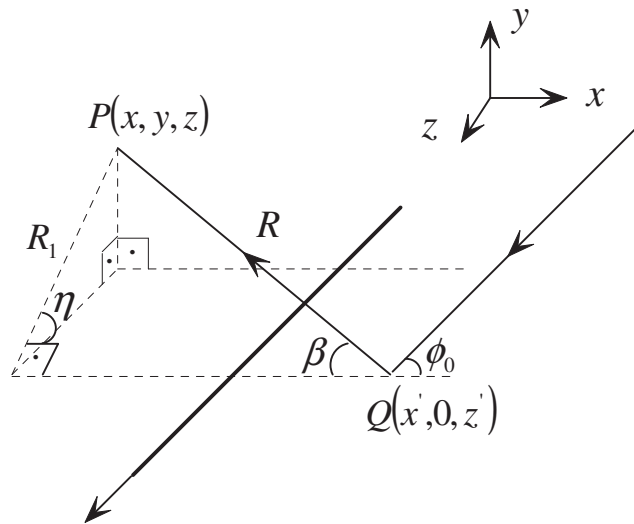
Figure 20 The geometry of the half-plane

The half-plane is illuminated by the plane wave of

$$\vec{H}_i = \vec{e}_z H_0 e^{jk(x\cos\phi_0 + y\sin\phi_0)} \tag{4.1}$$

where magnetic field polarization is taken into account and ϕ_0 is the incident angle. PO current is defined as

$$\vec{J}_{PO} = 2\vec{n} \times \vec{H}_i \Big|_s \qquad (4.2)$$

where $\vec{n}$ is the unit normal vector of the half plane and equal to $\vec{e}_y$. Magnetic vector potential is written as

$$\vec{A} = \frac{\mu_0}{4\pi} \iint_s \vec{J}_{PO} \frac{e^{-jkR}}{R} dS' \qquad (4.3)$$

The connection between the magnetic vector potential and the scattered magnetic field can be satisfied by

$$\vec{H} = \frac{1}{\mu_0} \nabla \times \vec{A} \qquad (4.4)$$

PO current is written as

$$\vec{J}_{PO} \Big|_s = \vec{e}_x 2H_0 e^{jkx' \cos \phi_0} \qquad (4.5)$$

with using Eq. (4.2) and Eq. (4.4). Scattering integral can be composed as

$$\vec{H} = \frac{H_0}{2\pi} \int\limits_{z'=-\infty}^{\infty} \int\limits_{x'=0}^{\infty} e^{jkx' \cos \phi_0} \nabla \times \left(\vec{e}_x \frac{e^{-jkR}}{R} \right) dx' dz' \qquad (4.6)$$

with using Eq. (4.3), Eq. (4.4) and Eq. (4.5) where R is the ray path and equal to $\left[(x-x')^2 + y^2 + (z-z')^2 \right]^{1/2}$. The curl operation in Eq. (4.6) is given as

$$\nabla \times \left(\vec{e}_x \frac{e^{-jkR}}{R} \right) = -\vec{e}_y \frac{jk(z-z')}{R} \frac{e^{-jkR}}{R} + \vec{e}_z jk \frac{y}{R} \frac{e^{-jkR}}{R} \qquad (4.7)$$

and from the Fig. 14 Eq. (4.7) is decomposed as

$$\nabla \times \left(\vec{e}_x \frac{e^{-jkR}}{R} \right) = -\vec{e}_y jk \cos \eta \sin \beta \frac{e^{-jkR}}{R} + \vec{e}_z jk \sin \eta \sin \beta \frac{e^{-jkR}}{R} \qquad (4.8)$$

where $\cos \eta = \dfrac{z-z'}{R_1}$, $\sin \beta = \dfrac{R_1}{R}$ and $\sin \eta = \dfrac{y}{R_1}$ respectively. Hence the Eq. (4.6) is decomposed as

$$\vec{H} = \frac{H_0}{2\pi} \int\limits_{z'=-\infty}^{\infty} \int\limits_{x'=0}^{\infty} e^{jkx' \cos \phi_0} \left(-\vec{e}_y jk \cos \eta \sin \beta + \vec{e}_z \sin \eta \sin \beta \right) \frac{e^{-jkR}}{R} dx' dz' \qquad (4.9)$$

according to the Eq. (4.8). x' part of the Eq. (4.9) can be taken by using the well-known edge point technique. The edge point technique is given as

$$\int_a^\infty f(x)e^{-jkg(x)}dx = \frac{1}{jk}f(a)\frac{1}{g'(a)}e^{-jkg(a)}$$ (4.10)

The phase function of the diffraction integral is written as

$$\psi = x'\cos\phi_0 - R$$ (4.11)

where the first derivative ψ' is equal to $\cos\phi_0 + \dfrac{x - x'}{R}$. The amplitude function is written as

$$f(x) = \frac{\cos\eta\sin\beta}{R}$$ (4.12)

At the $x' = 0$ point the phase function and its derivative takes the form as

$$\psi = R_e$$ (4.13)

and

$$\psi' = \cos\phi_0 - \cos\beta_e$$ (4.14)

where R_e is the ray path at the $x' = 0$ and equal to $\left[\rho^2 + (z - z')^2\right]^{\frac{1}{2}}$. The amplitude function takes the form as

$$f(x' = 0) = \frac{\cos\eta\sin\beta_e}{R_e}$$ (4.15)

Hence the diffraction integral takes the form as

$$\vec{H} = \frac{H_0}{2\pi}\int_{z'=-\infty}^{\infty}\left(-\vec{e}_y\cos\eta\sin\beta_e + \vec{e}_z\sin\eta\sin\beta_e\right)\frac{1}{\cos\phi_0 - \cos\beta_e}\frac{e^{-jkR_e}}{R_e}dz'$$ (4.16)

with using Eq. (4.13), (4.14) and Eq. (4.15). The stationary phase method can be used for the evaluation of the z' part of the diffraction integral. The phase function of the integral is written as

$$\psi = R_e$$ (4.17)

where the first derivative of the phase function is equal to $-\dfrac{z - z'}{R_e}$. The stationary phase point can be found by equating the first derivative of the phase function to zero. Then stationary phase point is found as

$$z_s = z.$$ (4.18)

At the stationary phase point η and β_e values are equal to $\dfrac{\pi}{2}$ and $\pi - \phi$, respectively. The second derivative of the phase function is written as

$$\psi'' = -\frac{-R_e^2 + (z - z')}{R_e^3} \tag{4.19}$$

, and it is equal to $\dfrac{1}{R_e}$ at the stationary phase point. The amplitude function can be written as

$$f(z' = z) = \frac{\sin \phi_0}{\cos \phi_0 + \cos \phi} \frac{1}{\rho} \tag{4.20}$$

at the stationary phase point. Hence, PO diffracted magnetic field is written as

$$\vec{H}_d^{PO} = \vec{e}_z \frac{H_0}{\sqrt{2\pi}} e^{-j\frac{\pi}{4}} \frac{\sin \phi}{\cos \phi + \cos \phi_0} \frac{e^{-jk\rho}}{\sqrt{k\rho}} \tag{4.21}$$

Exact diffracted field from the half plane is written as

$$\vec{H}_d = -\vec{e}_z H_0 \frac{e^{-j\frac{\pi}{4}}}{2\sqrt{2\pi}} \left(\frac{1}{\cos \dfrac{\phi - \phi_0}{2}} + \frac{1}{\cos \dfrac{\phi + \phi_0}{2}} \right) \frac{e^{-jk\rho}}{\sqrt{k\rho}} \tag{4.22}$$

Equation (4.22) is rearranged as

$$\vec{H}_d = -\vec{e}_z H_0 \frac{e^{-j\frac{\pi}{4}}}{\sqrt{2\pi}} \frac{2\cos \dfrac{\phi}{2} \cos \dfrac{\phi_0}{2}}{\cos \phi + \cos \phi_0} \frac{e^{-jk\rho}}{\sqrt{k\rho}} \tag{4.23}$$

The difference of the exact diffracted field and PO diffracted field can be found as

$$\vec{H}_f = -\vec{e}_z \frac{e^{-j\frac{\pi}{4}}}{\sqrt{2\pi}} \frac{2\cos \dfrac{\phi}{2} \cos \dfrac{\phi_0}{2} - \sin \phi}{\cos \phi + \cos \phi_0} \frac{e^{-jk\rho}}{\sqrt{k\rho}} \tag{4.24}$$

where $\vec{H}_f$ is found to be fringe field. A new coordinate system and other related angles are given in the Fig. 21 to generalize the magnetic fringe current.
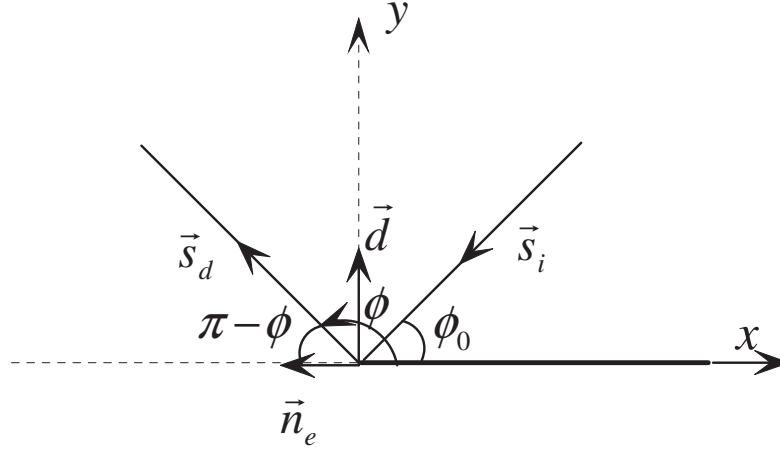
Figure 21 The geometry of the related angles

The following relations are written as

$$\cos\phi = -\vec{s}_d \cdot \vec{n}_e , \sin\phi = \vec{s}_d \cdot \vec{d} \tag{4.25}$$

$$\cos\phi_0 = \vec{s}_i \cdot \vec{n}_e \tag{4.26}$$

and

$$\cos\frac{\phi}{2} = \frac{1}{\sqrt{2}}\sqrt{1 - \vec{s}_d \cdot \vec{n}_e} \tag{4.27}$$

$$\cos\frac{\phi_0}{2} = \frac{1}{\sqrt{2}}\sqrt{1 + \vec{s}_i \cdot \vec{n}_e} \tag{4.28}$$

from the kinds of direction vectors. The expression of the fringe field is found as

$$\vec{H}_f = -\vec{e}_z \frac{e^{-j\frac{\pi}{4}}}{\sqrt{2\pi}} \frac{\sqrt{1 + \vec{s}_i \cdot \vec{n}_e}\sqrt{1 - \vec{s}_d \cdot \vec{n}_e} - \vec{s}_d \cdot \vec{d}}{(\vec{s}_i - \vec{s}_d) \cdot \vec{n}_e} \frac{e^{-jk\rho}}{\sqrt{k\rho}} \tag{4.29}$$

in terms of the direction vector. Hence, generalized magnetic fringe integral expression is defined as

$$\vec{H}_f = -\vec{e}_z \frac{1}{2\pi} \int_C H_i(Q_e) \frac{\sqrt{1 + \vec{s}_i \cdot \vec{n}_e}\sqrt{1 - \vec{s}_d \cdot \vec{n}_e} - \vec{s}_d \cdot \vec{d}}{(\vec{s}_i - \vec{s}_d) \cdot \vec{n}_e} \frac{e^{-jkR_e}}{R_e} dl . \tag{4.30}$$

4.2 Parabolic Reflector Application

The geometry of the problem is presented in the Fig. 22 where $\phi^{'}$ is the angle of incidence, ρ is the distance between the source and observation points, $\rho^{'}$ is the distance between the source and the reflector, $\vec{n}$ is the unit normal vector, R is the

ray path and P, Q are the observation and reflection points respectively. The angle between $\vec{n}$ and ρ' is equal to $\dfrac{\phi'}{2}$. f is the focal length of the PEC reflector. The PEC cylindrical reflector is lying between the angles $-\phi_0$ and ϕ_0.
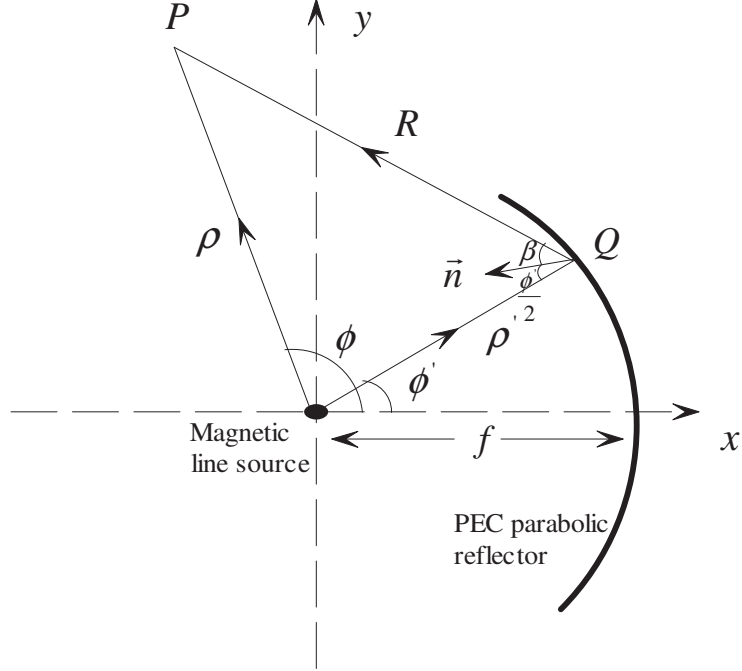
Figure 22 The geometry of parabolic reflector, which is illuminated by the magnetic line source

As can be seen from Fig. 22 parabolic reflector is fed by the magnetic line source which is defined as

$$\vec{H}_i = \vec{e}_z I_m \frac{e^{-jk\rho}}{\sqrt{k\rho}} \tag{4.31}$$

where I_m is the complex amplitude factor. PO electric current can be written directly as

$$\vec{J}_{PO} = 2\left(\cos\frac{\phi'}{2} \vec{e}_\phi + \sin\frac{\phi'}{2} \vec{e}_\rho \right) I_m \frac{e^{-jk\rho'}}{\sqrt{k\rho'}} \tag{4.32}$$

where $\vec{n}$ is the unit normal vector which is defined in Eq. (4.2) and equal to $-\cos\dfrac{\phi'}{2}\vec{e}_\rho + \sin\dfrac{\phi'}{2}\vec{e}_\phi$ for the problem geometry. Scattered magnetic field is written as

$$\vec{H}_{PO} = \frac{I_m}{2\pi} \iint_{s'} \nabla \times \left(\vec{e}_\phi \cos\frac{\phi'}{2} \frac{e^{-jkR}}{R} + \vec{e}_\rho \sin\frac{\phi'}{2} \frac{e^{-jkR}}{R} \right) \frac{e^{-jk\rho'}}{\sqrt{k\rho'}} dS' \qquad (4.33)$$

from expressions of Eq. (4.3), (4.4) and Eq. (4.31). R is the ray path and equal to

$\left[\rho^2 + \rho'^2 - 2\rho\rho' \cos(\phi - \phi') + (z - z')^2 \right]^{\frac{1}{2}}$ where ρ' is equal to $\dfrac{f}{\cos^2 \dfrac{\phi'}{2}}$. The curl

operation of the Eq. (4.33) is written as

$$\frac{1}{\rho}\left(\vec{e}_z \left(\cos\frac{\phi'}{2}\frac{e^{-jkR}}{R} - \cos\frac{\phi'}{2} jk \frac{e^{-jkR}}{R}\frac{\partial R}{\partial \rho} + \sin\frac{\phi'}{2} jk \frac{e^{-jkR}}{R}\frac{\partial R}{\partial \phi} \right) \right) \qquad (4.34)$$

where the derivatives of the ray path according to the ρ and ϕ are equal to

$\dfrac{\rho - \rho' \cos(\phi - \phi')}{R}$ and $\dfrac{\rho\rho' \sin(\phi - \phi')}{R}$ respectively. The angle equalities of the

derivative values can be written as

$$\frac{\partial R}{\partial \rho} = \cos\left(\phi - \frac{\phi'}{2} + \beta \right) \qquad (4.35)$$

and

$$\frac{\partial R}{\partial \phi} = \sin\left(\phi - \frac{\phi'}{2} + \beta \right) \qquad (4.36)$$

from Fig. 22. The angle equalities are inserted in to Eq. (4.34) and rearranged form of Eq. (4.34) is written as

$$\vec{e}_z \left\{ \frac{e^{-jkR}}{R}\left(\frac{1}{\rho}\cos\frac{\phi'}{2} + jk\cos(\phi - \phi' + \beta) \right) \right\} \qquad (4.40)$$

to be the end of the curl operation. Eq. (4.33) is rewritten as

$$\vec{H}_{PO} = \vec{e}_z \frac{I_m}{2\pi} \int_{z'=-\infty}^{\infty} \int_{\phi'=-\phi_0}^{\phi_0} \frac{e^{-jk\rho'}}{\sqrt{k\rho'}}\left(\frac{1}{\rho}\cos\frac{\phi'}{2} + jk\cos(\phi - \phi' + \phi) \right)\frac{e^{-jkR}}{R}\rho' d\phi' dz' \qquad (4.41)$$

with using Eq. (4.33) and Eq. (4.40). The z' part of the integral can be eliminated by using

$$\int_c e^{-jkR_1 ch\alpha} d\alpha = \frac{\pi}{j} H_0^{(2)}(kR_1) \qquad (4.42)$$

where $z - z' = R_1 sh\alpha$ and $R = \left[R_1^2 + (z - z')^2 \right]^{\frac{1}{2}}$. Hence, Eq. (4.41) is written as

$$\vec{H}_{PO} = \vec{e}_z \frac{I_m}{2j} \int_{\phi'=-\phi_0}^{\phi_0} \frac{e^{-jk\rho'}}{\sqrt{k\rho'}} \left(\frac{1}{\rho} \cos\frac{\phi'}{2} + jk\cos(\phi - \phi' + \beta) \right) H_0^{(2)}(kR_1)\rho' d\phi' \quad (4.43)$$

with respect to the Eq. (4.42). The effect of the edges of the parabolic reflector can be found by applying the fringe field expression. The geometry of the diffracted field is given in Fig. 23.
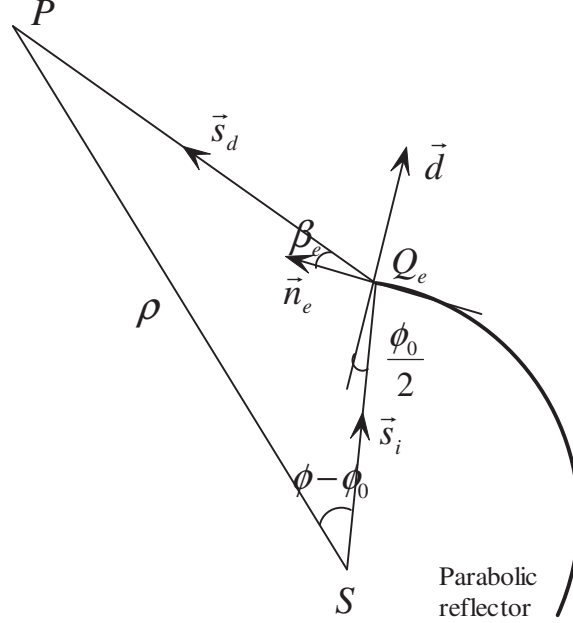
Figure 23 The geometry of diffracted fields

The related expressions are defined as

$$\vec{s}_i = \vec{d} \cos\frac{\phi_0}{2} + \vec{n}_e \sin\frac{\phi_0}{2} \quad (4.44)$$

and

$$\vec{s}_d = \vec{n}_e \cos\beta_e + \vec{d} \sin\beta_e \sin\eta \quad (4.45)$$

where $\vec{d} = \vec{e}_\rho \cos\frac{\phi_0}{2} + \vec{e}_\phi \sin\frac{\phi_0}{2}$ and $\vec{n}_e = \vec{e}_\rho \sin\frac{\phi_0}{2} - \vec{e}_\phi \cos\frac{\phi_0}{2}$ for the upper edge. When the Eq. (4.44) and Eq. (4.45) are inserted to the Eq. (4.30), the fringe field expression is written as

$$\vec{H}_f^u = -\vec{e}_z \frac{1}{2\pi} \int_{z'=-\infty}^{\infty} I_m \frac{e^{-jk\rho_0}}{\sqrt{k\rho_0}} \frac{\sqrt{1+\sin\frac{\phi_0}{2}}\sqrt{1-\cos\beta_e} - \sin\beta_e \sin\eta}{\sin\frac{\phi_0}{2} - \cos\beta_e} \frac{e^{-jkR_e}}{R_e} dz' \quad (4.46)$$

where R_e is the ray path and equal to $\left[\rho^2 + \rho_0^2 - 2\rho\rho_0 \cos(\phi - \phi_0) + (z - z')^2 \right]^{1/2}$. The phase function is written as

$$\psi = R_e \tag{4.47}$$

where the first derivative of the phase function is equal to $\psi' = -\dfrac{z - z'}{R_e}$. Stationary phase point can be found by equating the first derivative of the phase function to zero. Hence, the stationary phase point z'_s is equal to z. The second derivative of the phase function can be written as

$$\psi''_s = \frac{1}{R_{es}} \tag{4.48}$$

at the stationary phase point where R_{es} is equal to $\left[\rho^2 + \rho_0^2 - 2\rho\rho_0 \cos(\phi - \phi_0)\right]^{\frac{1}{2}}$. The amplitude function is written as

$$f\left(z'_s = z\right) = \frac{\sqrt{1 + \sin\dfrac{\phi_0}{2}}\sqrt{1 - \cos\beta_{es}} - \sin\beta_{es}\sin\eta_s}{\sin\dfrac{\phi_0}{2} - \cos\beta_{es}}\frac{1}{R_{es}} \tag{4.49}$$

at the stationary phase point. Hence, Eq. (4.46) can be rewritten as

$$\vec{H}^u_f = -\vec{e}_z \frac{I_m}{\sqrt{2\pi}} \frac{e^{-jk\rho_0}}{\sqrt{k\rho_0}} e^{-j\frac{\pi}{4}} \frac{\sqrt{1 + \sin\dfrac{\phi_0}{2}}\sqrt{1 - \cos\beta_{es}} - \sin\beta_{es}\sin\eta_s}{\sin\dfrac{\phi_0}{2} + \cos\beta_{es}}\frac{e^{-jkR_{es}}}{\sqrt{kR_{es}}} \tag{4.50}$$

where the β_{es} and η_s is equal to $\pi - \phi$ and $\dfrac{\pi}{2}$ respectively. The related expressions for the lower edge of the PEC cylindrical reflector is defined as

$$\vec{s}_i = \vec{d}\cos\frac{\phi_0}{2} + \vec{n}_e \sin\frac{\phi_0}{2} \tag{4.51}$$

and

$$\vec{s}_d = \vec{n}_e \cos\beta_e + \vec{d}\sin\beta_e \sin\eta \tag{4.52}$$

where $\vec{d} = \vec{e}_\rho \cos\dfrac{\phi_0}{2} + \vec{e}_\phi \cos\dfrac{\phi_0}{2}$ and $\vec{n}_e = -\vec{e}_\rho \sin\dfrac{\phi_0}{2} + \vec{e}_\phi \cos\dfrac{\phi_0}{2}$ for the lower edge. Eq. (4.30) is written as

$$\vec{H}^l_f = \vec{e}_z \frac{I_m}{2\pi} \frac{e^{-jk\rho_0}}{\sqrt{k\rho_0}} \int_{z=-\infty}^{\infty} \frac{\sqrt{1 + \sin\dfrac{\phi_0}{2}}\sqrt{1 - \cos\beta_e} - \sin\beta_e \sin\eta}{\sin\dfrac{\phi_0}{2} - \cos\beta_e}\frac{e^{-jkR_e}}{R_e}dz \tag{4.53}$$

for the lower edge where R_e is equal to $\left[\rho^2 + \rho_0^2 - 2\rho\rho_0 \cos(\phi + \phi_0) + (z - z')^2\right]^{1/2}$.

The phase function of Eq. (4.53) is written as

$$\psi = R_e \tag{4.54}$$

and its first derivative ψ' is equal to $-\dfrac{z - z'}{R_e}$. The stationary phase point can be

found as $z_s' = z$ by equating the first derivative of the phase function to zero. The

second derivative of the phase function is written as

$$\psi_s'' = \frac{1}{R_{es}} \tag{4.55}$$

at the stationary phase point and R_{es} is equal to $\left[\rho^2 + \rho_0^2 - 2\rho\rho_0 \cos(\phi + \phi_0)\right]^{1/2}$. The

value of the amplitude function is written as

$$f\left(z_s' = z\right) = \frac{\sqrt{1 + \sin\dfrac{\phi_0}{2}}\sqrt{1 - \cos\beta_{es}} - \sin\beta_{es}\sin\eta_s}{\sin\dfrac{\phi_0}{2} - \cos\beta_{es}} \frac{1}{R_{es}} \tag{4.56}$$

at the stationary phase point and the values of the angles β_{es}, η_s are equal to $\pi - \phi$

and $\dfrac{\pi}{2}$, respectively. Hence, Eq. (4.53) is rewritten as

$$\vec{H}_f^l = -\vec{e}_z \frac{I_m}{\sqrt{2\pi}} \frac{e^{-jk\rho_0}}{\sqrt{k\rho_0}} e^{-j\frac{\pi}{4}} \frac{\sqrt{1 + \sin\dfrac{\phi_0}{2}}\sqrt{1 - \cos\beta_{es}} - \sin\beta_{es}}{\sin\dfrac{\phi_0}{2} - \cos\beta_{es}} \frac{e^{-jkR_{es}}}{\sqrt{kR_{es}}} \tag{4.57}$$

The exact diffracted field can be found as

$$\vec{H}_E = \vec{H}_{PO} + \vec{H}_f^u + \vec{H}_f^l \tag{4.58}$$

by adding the contributions of the fringe fields to the PO diffracted field.

4.3 Numerical Results

In this analysis part, exact diffracted fields, fringe fields and diffracted PO fields will

be investigated. In order to investigate the far field radiation, the observation distance

is taken reasonably away from the scatterer. The observation distance will be taken

as 7λ, where λ is the wavelength, and The focal length f will be taken as 2λ. The parabolic reflector will be positioned between the angles $-\phi_0$ and ϕ_0.
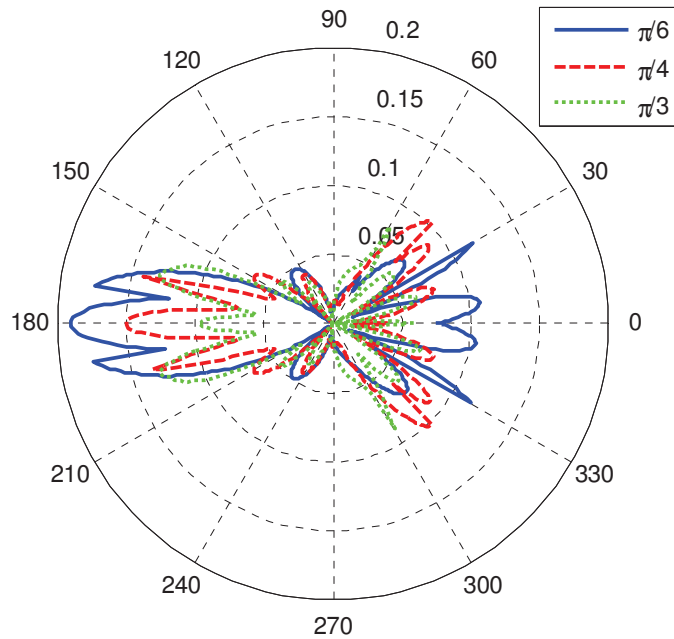
Figure 24 Exact diffracted fields

Figure 24 shows the exact diffracted fields from the edges of the parabolic reflector, which is given in the Eq. (4.58) for different incident angles. The amplitude values of the diffracted fields become dominant on the reflection region. The main beams can be observed between the angles 150° and 210°. The maximum radiation is observed at 180°. The fields' amplitudes take the minimum values at 90° and 270°. The effect of the incident angle ϕ_0 can be seen directly in Fig. 24. The diffracted fields' amplitudes decrease in the reflection region when the incident angle increases.
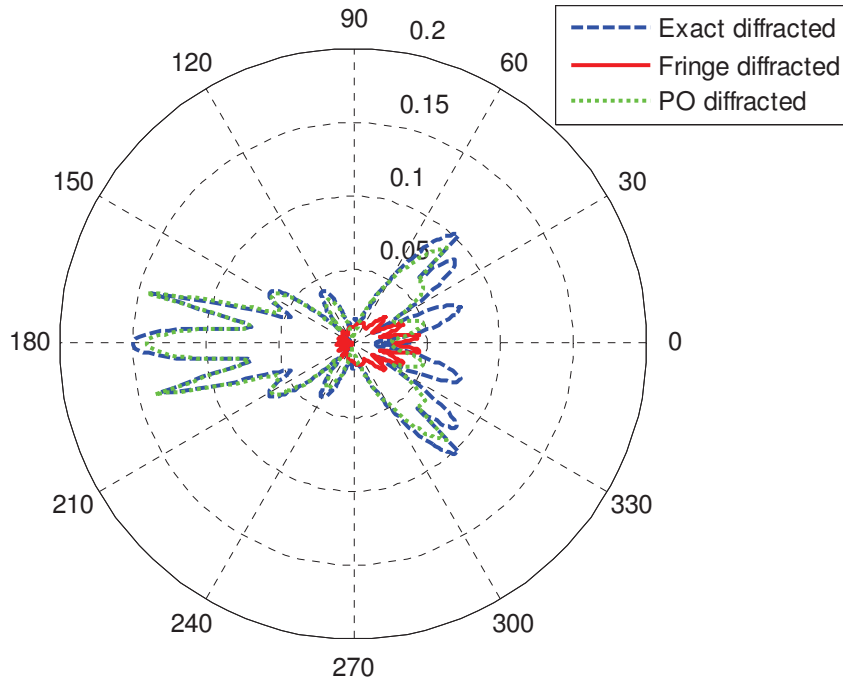
Figure 25 The PO, fringe and exact diffracted fields for $\phi_0 = \dfrac{\pi}{4}$

Figure 25 shows the exact, fringe and the PO diffracted fields. The PO diffracted field is in a perfect harmony with the exact diffracted field except for the reflection boundaries, which are at the angles 45° and 315° respectively. The PO and exact diffracted fields take maximum amplitude values at 180°. Although the PO diffracted fields amplitude goes to zero value at the 90° and 270°, exact diffracted fields take different amplitude values at those angles. The fringe diffracted fields' amplitude takes the major values between the reflection regions. The minor lobes are observed between the angles 90° and 270°. The fringe diffracted fields fix the defects of the PO diffracted fields in both reflection and shadow boundaries and also reflection and shadow regions.

CHAPTER 5

DIFFRACTION by AN IMPEDANCE HALF-PLANE

5.1 Introduction and Solution of the Problem

This part is based on the paper by Başdemir H. D., "*Fringe Waves in An Impedance Half-Plane*", Progress in Electromagnetic Research, vol. 138, pp. 571-584, (2013).

Uniform fringe field expression for an impedance half-plane will be obtained in this chapter. In the beginning, PO expression for the half-plane geometry will be obtained from Huygens-Kirchhoff integral under the impedance boundary condition. The geometry of the problem is given in Fig. 26. The half-plane is lying on the surface $\{x \in [0,\infty), y = 0, z \in (-\infty,\infty)\}$.

Figure 26 The geometry of an impedance half-plane
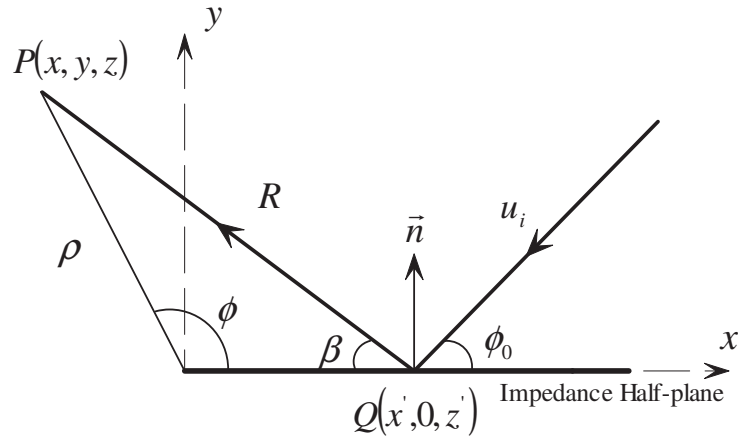
We consider the E-polarization case for the incident field in this study. The method can also be applied to the H-polarization case. The half-plane is illuminated by the plane-wave of

$$u_i = u_0 e^{jk(x\cos\phi_0 + y\sin\phi_0)} \tag{5.1}$$

where the u_0 is the complex amplitude factor and u_i is any component of the electric field. The total field can be written as

$$u_t = u_i + u_r \tag{5.2}$$

where u_r is the reflected field from the surface. The PO takes the reflected fields as a geometric optics (GO) fields so the reflected field can be described as

$$u_r = \Gamma u_0 e^{jk(x\cos\phi_0 - y\sin\phi_0)} \tag{5.3}$$

where Γ is the reflection coefficient and equal to

$$\Gamma = \frac{\sin\phi_0 - \sin\theta}{\sin\phi_0 + \sin\theta} \tag{5.4}$$

according to Ref. [57]. When taking into account the reflection coefficient which is given in Eq. (5.4) the angle θ determines the surfaces polarization case. When $\sin\theta$ takes the values between one and infinity, electric polarization case is observed, and if $\sin\theta$ takes the values between zero and one, magnetic polarization case is observed.

The Eq. (5.2) is rearranged according to Eq. (5.1) and Eq. (5.3), (5.4) and redefined on the scattering surface as

$$u_t\big|_{y'=0} = (1+\Gamma)u_0 e^{jkx'\cos\phi_0} . \tag{5.5}$$

The impedance boundary condition for the Cartesian coordinates is defined as

$$u_t\big|_s = \frac{1}{jk\sin\theta}\frac{\partial u_t}{\partial n}\bigg|_s \tag{5.6}$$

where s is the $y = 0$ plane, n is the unit normal vector of the scattering surface, $\sin\theta$ is equal to $\dfrac{Z_0}{Z}$, and Z_0 is the impedance of the vacuum, and Z is the impedance of the scatterer. According to Eq. (5.5) and Eq. (5.6), derivative of the field expression is written as

$$\frac{\partial u_t}{\partial y'}\bigg|_{y'=0} = \frac{2jku_0\sin\theta\sin\phi_0}{\sin\phi_0 + \sin\theta}e^{jkx'\cos\phi_0} . \tag{5.7}$$

For the 2-D case, if the geometry is symmetric according to the z' coordinates a further expression of the Huygens-Kirchhoff integral can be given by

$$u(P) = \frac{1}{4\pi}\int_l \left(u\frac{\partial G}{\partial n} - G\frac{\partial u}{\partial n}\right)dl' \tag{5.8}$$

where P is the observation point and G is the Green's function. The 2-D Green's function is given as

$$G = \frac{\pi}{j} H_0^{(2)}(kR) \tag{5.9}$$

The PO integral is constructed as

$$u_{PO}(P) = \frac{2u_0 \sin\phi_0}{4\pi} \int\limits_{x'=0}^{\infty} \left(\frac{1}{\sin\phi_0 + \sin\theta} e^{jkx'\cos\phi_0} \frac{\partial G}{\partial y'} - \frac{jk\sin\theta}{\sin\phi_0 + \sin\theta} e^{jkx'\cos\phi_0} G \right) dx' \tag{5.10}$$

according to Eq. (5.5), (5.7), (5.8) and the geometry of the problem. The term $\dfrac{\partial G}{\partial y'}$

can be found from the chain rule as

$$\frac{\partial G}{\partial y'} \cong \frac{\pi}{j} \frac{\partial H_0^{(2)}(kR)}{\partial R} \frac{\partial R}{\partial y'} \tag{5.11}$$

where R is the ray path and equal to $\left[(x-x')^2 + (y-y')^2 \right]^{1/2}$. The derivative operation of the ray path according to the normal vector is written as

$$\left. \frac{\partial R}{\partial y'} \right|_{y'=0} = -\frac{y}{R} \tag{5.12}$$

where $-\dfrac{y}{R}$ is written as $-\sin\beta$ from the geometry of the problem. The Eq. (5.11) is

obtained

$$\frac{\partial G}{\partial y'} \cong \frac{k\pi}{j} H_1^{(2)}(kR)\sin\beta \tag{5.13}$$

by inserted Eq. (5.12) into Eq. (5.11) and the derivative operation $\dfrac{\partial H_0^{(2)}(kR)}{\partial R}$ is equal

to $-kH_1^{(2)}(kR)$. Therefore, the PO integral which is given in Eq. (5.10) is reconstructed as

$$u_{PO}^d(P) = \frac{1}{2} \frac{ku_0 \sin\phi_0}{\sin\phi_0 + \sin\theta} \int\limits_{x'=-\infty}^{\infty} (\sin\beta - \sin\theta) e^{jkx'\cos\phi_0} H_1^{(2)}(kR_1) dx' \tag{5.14}$$

where R_1 is the ray path and equal to $\left[(x-x')^2 + y^2 \right]^{1/2}$. Debby asymptotic expansion of the Hankel function is written as

$$H_1^{(2)}(kR_1) \approx \sqrt{\frac{2}{\pi k R_1}} e^{-jkR_1} e^{j\frac{3\pi}{4}} \tag{5.15}$$

where $kR_1 \gg 1$. As a result the Eq. (5.14) yields

$$u_{PO}(P) = \frac{ku_0 \sin\phi_0}{\sin\phi_0 + \sin\theta} \frac{e^{j\frac{\pi}{4}}}{\sqrt{2\pi}} \int_{x'=0}^{\infty} (\sin\beta - \sin\theta)e^{jkx'\cos\phi_0} \frac{e^{jkR_1}}{\sqrt{kR_1}} dx' \qquad (5.16)$$

where R_1 is equal to $\left[(x-x')^2 + y^2\right]^{1/2}$. The integral expression can be transformed into

$$u_{PO}(P) = \frac{ku_0 \sin\phi_0}{\sin\phi_0 + \sin\theta} \frac{e^{j\frac{\pi}{4}}}{\sqrt{2\pi}} \int_{x'=0}^{\infty} \frac{1}{\sin\phi_0} \left[\cos\frac{\beta+\phi_0}{2} \sin\frac{\beta-\phi}{2} \right.$$

$$\left. - \cos\frac{\beta-\phi_0}{2} \sin\frac{\beta+\phi}{2} \right] (\sin\beta - \sin\theta)e^{jkx'\cos\phi_0} \frac{e^{-jkR_1}}{\sqrt{kR_1}} dx' \qquad (5.17)$$

by using Ref. [11] for separately investigation of the incident and reflected diffracted fields by using the trigonometric relation of $\sin(a-b) = \sin a\cos b - \cos a\sin b$. The incident and reflected diffracted fields can be written as

$$u_{PO}^{id}(P) = \frac{ku_0}{\sin\phi_0 + \sin\theta} \frac{e^{j\frac{\pi}{4}}}{\sqrt{2\pi}} \int_{x'=0}^{\infty} (\sin\beta - \sin\theta)\cos\frac{\beta+\phi_0}{2}$$

$$\times \sin\frac{\beta-\phi}{2} e^{jkx'\cos\phi_0} \frac{e^{-jkR_1}}{\sqrt{kR_1}} dx' \qquad (5.18)$$

and

$$u_{PO}^{rd}(P) = -\frac{ku_0}{\sin\phi_0 + \sin\theta} \frac{e^{j\frac{\pi}{4}}}{\sqrt{2\pi}} \int_{x'=0}^{\infty} (\sin\beta - \sin\theta)\cos\frac{\beta-\phi_0}{2}$$

$$\times \sin\frac{\beta+\phi}{2} e^{jkx'\cos\phi_0} \frac{e^{-jkR_1}}{\sqrt{kR_1}} dx' \qquad (5.19)$$

respectively. The asymptotic evaluation of Eq. (5.18) can be found by using the edge point technique. The edge point technique is given as

$$\int_{x}^{\infty} f(\alpha)e^{jkg(\alpha)}d\alpha \cong -\frac{1}{jk} \frac{f(x)}{g'(x)} e^{jkg(x)} \qquad (5.20)$$

where the detailed explanation can be found in Ref. [11]. The phase function of Eq. (5.18) is written as

$$g(x') = x'\cos\phi_0 - R_1. \qquad (5.21)$$

The first derivative of the phase function can be found as

$$g'(x') = \cos\phi_0 + \frac{x-x'}{R_1}. \tag{5.22}$$

The stationary phase values of the phase functions are found as

$$g(x_e) = -\rho \tag{5.23}$$

and

$$g'(x_e) = \cos\phi_0 + \frac{x}{R_1} \tag{5.24}$$

where $\dfrac{x}{R_1}$ is written as $-\cos\beta_e$ from the geometry of the problem and keep in mind

that β_e which is the reflection angle's value at the edge is equal to $\pi-\phi$. The

amplitude function can be written as

$$f(x_e) = (\sin\beta_e - \sin\theta)\cos\frac{\beta_e+\phi_0}{2}\sin\frac{\beta_e-\phi_0}{2}\frac{1}{\sqrt{k\rho}} \tag{5.25}$$

at the edge. Hence, the asymptotic incident diffracted PO field is obtained as

$$u_{PO}^{id}(P) = -\frac{u_0}{\sin\phi_0+\sin\theta}\frac{e^{-j\frac{\pi}{4}}}{\sqrt{2\pi}}\frac{(\sin\phi-\sin\theta)\sin\dfrac{\phi-\phi_0}{2}\cos\dfrac{\phi+\phi_0}{2}}{\cos\phi_0+\cos\phi}\frac{e^{-jk\rho}}{\sqrt{k\rho}} \tag{5.26}$$

by using the edge point method. The Eq. (5.26) is simplified as

$$u_{PO}^{id}(P) = -\frac{u_0}{\sin\phi_0+\sin\theta}\frac{e^{-j\frac{\pi}{4}}}{\sqrt{2\pi}}\frac{(\sin\phi-\sin\theta)\sin\dfrac{\phi-\phi_0}{2}}{2\cos\dfrac{\phi-\phi_0}{2}}\frac{e^{-jk\rho}}{\sqrt{k\rho}} \tag{5.27}$$

using the trigonometric relation of $\cos a + \cos b = 2\cos\dfrac{a+b}{2}\cos\dfrac{a-b}{2}$. The

diffracted field, in Eq. (5.27) is not uniform since it approaches to infinity at the

shadow and reflection boundaries. The uniform theory is based on the asymptotic

relation of

$$sign(x)F[|x|] \cong \frac{e^{-j\frac{\pi}{4}}}{2\sqrt{\pi}}\frac{e^{-jx^2}}{x} \tag{5.28}$$

for $x \gg 1$ [58-59]. The $sign(x)$ is the signum function which is equal to 1 for $x > 0$

and -1 for $x < 0$. The $F[x]$ is the Fresnel function and can be defined by the integral

of

$$F[x] = \frac{e^{j\frac{\pi}{4}}}{\sqrt{\pi}} \int_x^\infty e^{-jy^2} dy. \tag{5.29}$$

In order to obtain the uniform version of the diffracted fields, two new parameters are introduced as

$$\xi_- = -\sqrt{2k\rho} \cos\frac{\phi - \phi_0}{2} \tag{5.30}$$

and

$$\xi_+ = -\sqrt{2k\rho} \cos\frac{\phi + \phi_0}{2} \tag{5.31}$$

for using instead of x in Eq. (5.28). Hence, the uniform version of the Eq. (5.27) can be obtained as

$$u_{PO}^{id}(P) = \frac{u_0}{\sin\phi_0 + \sin\theta}(\sin\phi - \sin\theta)\sin\frac{\phi - \phi_0}{2} e^{jk\rho\cos\phi - \phi_0} sign(\xi_-)F[|\xi_-|]. \tag{5.32}$$

The same procedure is valid for the reflected diffracted field, so the uniform version of the reflected diffracted field is directly written as

$$u_{PO}^{rd}(P) = -\frac{u_0}{\sin\phi_0 + \sin\theta}(\sin\phi - \sin\theta)\sin\frac{\phi + \phi_0}{2} e^{jk\rho\cos(\phi - \phi_0)} sign(\xi_+)F[|\xi_+|]. \tag{5.33}$$

If the scattering geometry is symmetric with respect to the z' coordinate, the generalized PO integral for an arbitrary impedance surface is written as

$$u_M(P) = -\frac{k}{2}\int_{l'} u(Q)_i q(\alpha, \pi - \beta)H_0^{(2)}(kR)dl' \tag{5.34}$$

from Ref. [60], where α is the incident angle, and β is the reflection angle. According to Fig. 20 Eq. (5.34) can be rewritten as

$$u_M(P) = \frac{-ku_0}{2}\int_{x'=-\infty}^\infty e^{jkx'\cos\phi_0} q(\phi_0, \pi - \beta)H_0^{(2)}(kR_1)dx' \tag{5.35}$$

where $q(\phi_0, \pi - \beta)$ is the compositions of the Maliuzhinetz function and is equal to

$$q(\phi_0, \pi - \beta) = \frac{\psi(\phi)}{\psi(\pi - \alpha)}\sin\frac{\alpha}{2}\left[\psi(-\phi)\left(\sin\frac{\phi}{2} - \cos\frac{\alpha}{2}\right)\right.$$

$$\left. + \psi(2\pi - \phi)\left(\sin\frac{\phi}{2} + \cos\frac{\alpha}{2}\right)\right] \tag{5.36}$$

where $\psi(x)$ is written as

$$\psi(x) = \psi_\pi\left(x + \frac{3\pi}{2} - \theta\right)\psi_\pi\left(x + \frac{\pi}{2} + \theta\right)$$

$$\times \psi_\pi\left(x - \frac{\pi}{2} - \theta\right)\psi_\pi\left(x - \frac{3\pi}{2} + \theta\right). \tag{5.37}$$

The term $\psi_\pi(x)$ is the Maliuzhinetz function and can be described as

$$\psi_\pi(x) = \exp\left(-\frac{1}{8\pi}\int_0^x \frac{\pi\sin\eta - 4\pi\cos\frac{\pi}{4}\sin\frac{\eta}{2} + 2\eta}{\cos\eta}d\eta\right). \tag{5.38}$$

Hence, using Debby asymptotic form of the $H_0^{(2)}(kR)$, which is equal to

$$H_0^{(2)}(kR) = \sqrt{\frac{2}{\pi}}e^{j\frac{\pi}{4}}\frac{e^{-jkR}}{\sqrt{kR}} \tag{5.39}$$

the scattering integral takes the form

$$u_M(P) = -u_0 k\frac{e^{j\frac{\pi}{4}}}{\sqrt{2\pi}}\int_{x'=0}^{\infty} e^{jkx'\cos\phi_0}q(\phi_0,\pi - \beta)\frac{e^{-jkR_1}}{\sqrt{kR_1}}dx' \tag{5.40}$$

where R_1 is the ray path and equal to $\left[(x - x')^2 + y^2\right]^{\frac{1}{2}}$. The phase function and the amplitude function of Eq. (5.40) are written as

$$g(x') = x'\cos\phi_0 - R_1 \tag{5.41}$$

and

$$f(x') = q(\phi_0,\pi - \beta)\frac{1}{\sqrt{kR_1}}. \tag{5.42}$$

The first derivative of the phase function is derived as

$$g'(x') = \cos\phi_0 - \frac{dR_1}{dx'} \tag{5.43}$$

where $\dfrac{dR_1}{dx'}$ can be found $\dfrac{x - x'}{R_1}$, and this expression is written as $-\cos\beta$ from the geometry of the problem. The edge point contribution of Eq. (5.40) can be obtained as

$$u_M(P) = u_0\frac{e^{-j\frac{\pi}{4}}}{\sqrt{2\pi}}q(\phi_0,\pi - \beta_e)\frac{1}{\sqrt{k\rho}}\frac{1}{\cos\phi_0 - \cos\beta_e}e^{-jk\rho} \tag{5.44}$$

by using the edge point technique which is given in Eq. (5.20). The reflection angle β takes β_e value in the edges and equal to $\pi - \phi$. The Eq. (5.44) is rewritten as

$$u_M(P) = u_0 \frac{e^{-j\frac{\pi}{4}}}{\sqrt{2\pi}} \frac{q(\phi_0, \phi)}{\cos\phi_0 + \cos\phi} \frac{e^{-jk\rho}}{\sqrt{k\rho}} \tag{5.45}$$

Equation (5.45) can be separated into incident and reflected diffracted part using the trigonometric relation, which is previously given. After the trigonometric separation operation, Eq. (5.45)'s uniform version can be written as

$$u_M^{rd}(P) = -\frac{q(\phi_0, \phi)}{\sin\phi_0} e^{jk\rho\cos(\phi+\phi_0)} \sin\frac{\phi+\phi_0}{2} sign(\xi_+) F\left[|\xi_+|\right] \tag{5.46}$$

and

$$u_M^{id}(P) = \frac{q(\phi_0, \phi)}{\sin\phi_0} e^{jk\rho\cos(\phi-\phi_0)} \sin\frac{\phi-\phi_0}{2} sign(\xi_-) F\left[|\xi_-|\right] \tag{5.47}$$

by using Eq. (5.28) and Eq. (5.29). According to the PTD, fringe fields can be obtained subtracting the PO fields from the exact solution, so the total fringe field expression can be obtained as

$$u_f(P) = u_M(P) - u_{PO}(P) \tag{5.48}$$

where the $u_M(P)$ is the exact edge diffracted fields expression from the impedance half plane and to be formed as

$$u_M(P) = u_M^{id}(P) + u_M^{rd}(P) \tag{5.49}$$

by the addition of Eq. (5.46), (5.47). Also $u_{PO}(P)$ is the edge contribution of the PO method and to be formed as

$$u_{PO}(P) = u_{PO}^{id}(P) + u_{PO}^{rd}(P) \tag{5.50}$$

by addition of Eqs. (5.32) and (5.33). The expressions of the incident and reflected diffracted fringe fields can be written as

$$u_f^{id}(P) = u_M^{id}(P) - u_{PO}^{id}(P) \tag{5.51}$$

and

$$u_f^{rd}(P) = u_M^{rd}(P) - u_{PO}^{rd}(P) \tag{5.52}$$

respectively, taking into account Eqs. (5.32), (5.33), (5.46) and Eq. (5.47). Equation (5.48) is valid for obtaining the asymptotic fringe field expression. In the beginning, asymptotic PO contribution can be obtained from the evaluation of Eq. (5.16)

according to Eq. (5.20). After this evaluation, the asymptotic PO field can be found as

$$u_{PO}^a(P) = -\frac{u_0 \sin \phi_0}{\sin \phi_0 + \sin \theta} \frac{e^{-j\frac{\pi}{4}}}{\sqrt{2\pi}} \frac{\sin \phi - \sin \theta}{\cos \phi_0 + \cos \phi} \frac{e^{-jk\rho}}{\sqrt{k\rho}}.$$ (5.53)

The asymptotic fringe field expression can written as

$$u_f^a(P) = \frac{u_0}{\cos \phi_0 + \cos \phi} \frac{e^{-j\frac{\pi}{4}}}{\sqrt{2\pi}} \left[q(\phi_0, \phi) + \frac{\sin \phi_0 (\sin \phi - \sin \theta)}{\sin \phi_0 + \sin \theta} \right] \frac{e^{-jk\rho}}{\sqrt{k\rho}}$$ (5.54)

using the subtraction of Eq. (5.53) from Eq. (5.45).

5.2 Numerical Results

In this section, fringe field expressions will be analyzed numerically. In order to investigate the far field radiation, the observation distance is taken reasonably away from the scatterer. The high frequency asymptotic techniques can be used under the condition of $k\rho \gg 1$, where ρ and k are the observation distance and wave numbers, respectively. The wave number k is equal to $\frac{2\pi}{\lambda}$, where λ is the wavelength. If the observation distance ρ is taken as 6λ, the high frequency condition is found as $12\pi \gg 1$, so the high-frequency condition is provided by the distance 6λ. The angle of incidence ϕ_0 is taken as 60° and the $\sin \theta$ term will be taken as 4. Although the function $\sin \theta$ takes values between -1 and 1 in trigonometry, in the literature for impedance boundary condition it can takes values from zero to infinity. It should not be confused with trigonometry. It has been used in this way in the literature since Maliuzhinetz [61]. Figure 27 shows the diffracted fringe fields where the expressions were given in Eq. (5.48), (5.51) and Eq. (5.52). It can be seen that a minor lobe occurs between the reflection and shadow boundaries and there is not any amplitude values at the reflection (120°) and shadow boundaries (240°). The major radiation is observed in the illuminated and the shadow regions. The amplitude variations of the incident diffracted fringe fields go to zero at 240°, and the amplitude variation of the reflected diffracted fringe fields goes to zero at 120°. Furthermore, it can be observed in Fig. 27 that incident diffracted fringe fields concentrate in the shadow regions so compensate the incident fields in the

illuminated regions, and also reflected diffracted fields concentrate in the illuminated regions to compensate the reflected fields in the shadow regions.
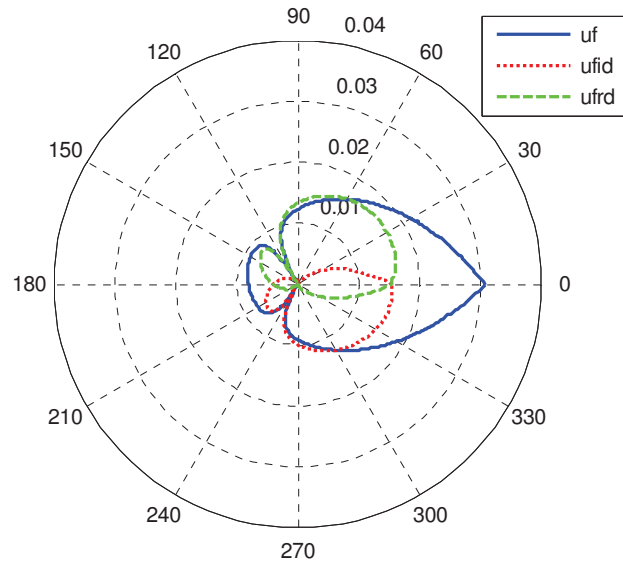

Figure 27 Total diffracted, incident diffracted and reflected diffracted fringe fields

Figure 28 shows the uniform and asymptotic fringe fields. The asymptotic fringe field expression is given in Eq. (5.54). Although the amplitudes take equal values in the illuminated and shadow regions, in the transition regions take different values. The asymptotic fringe field takes different than zero amplitude value at 120˚ and 240˚ when compared with the uniform fringe field. This is a predicted scene for the asymptotic fringe fields for an impedance structures. The reason of the enhancement at 120˚ is the result of the asymptotic expressions, which is given in the Eq. (5.54). In Fig. 28 this behavior is tried to explain. According to the PTD, asymptotic expression of the fringe field can be obtained subtraction of the PO asymptotic expression from the exact asymptotic solution. The asymptotic expressions give infinite values at the transition regions. Due to the uncertainty resulting from the extraction process, finite field values are obtained after this operation. Although the fields compensate to each other in all direction of observation, at the reflection boundary the fields can't compensate to each other so the enhancement at 120˚ is observed. Figure 29 shows that the asymptotic fringe field amplitude varies with the observation angle. In this case amplitude value takes more understandable at 120˚

(reflection boundary). This behavior is related to the reflection coefficient. Incident diffracted fields are independent of the surface reflection coefficient so at 240° there is no amplitude change in that region.
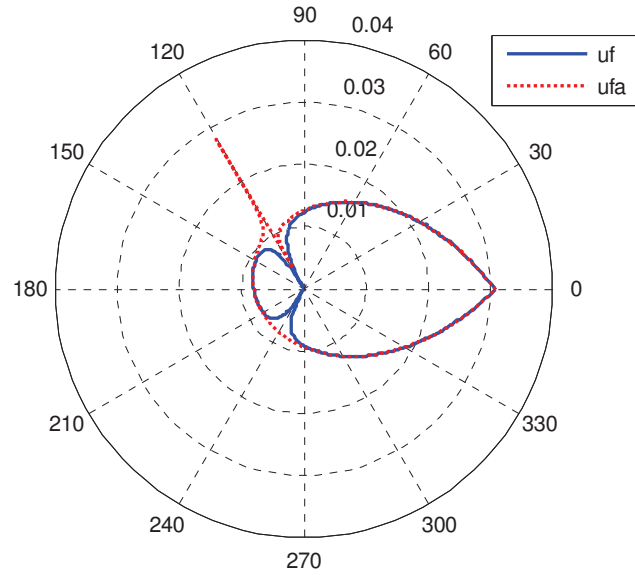
Figure 28 Uniform and non-uniform fringe fields

In the reflection coefficient when $\sin\theta$ approaches to infinity in Eq. (5.54), surface acts as a perfectly conducting surface. It can be seen from Fig. 23 that the reflected diffracted fringe field's amplitudes will become equal point with respect to the incident diffracted fields. Therefore at 120° and 240° amplitudes take equal values. The amplitude values for all plots were found as expected because diffracted fields compensate the deficiencies of the GO fields in the transition regions and take half of the amplitude values of the GO fields.

Figure 29 The asymptotic fringe field when $\sin\theta \rightarrow \infty$

CHAPTER 6

CONCLUSION

In this thesis, fringe field's contributions to the scattered fields were investigated for different geometries. Initially cylindrical structures are investigated taking into account the PEC and impedance boundary conditions. The PEC cylinder 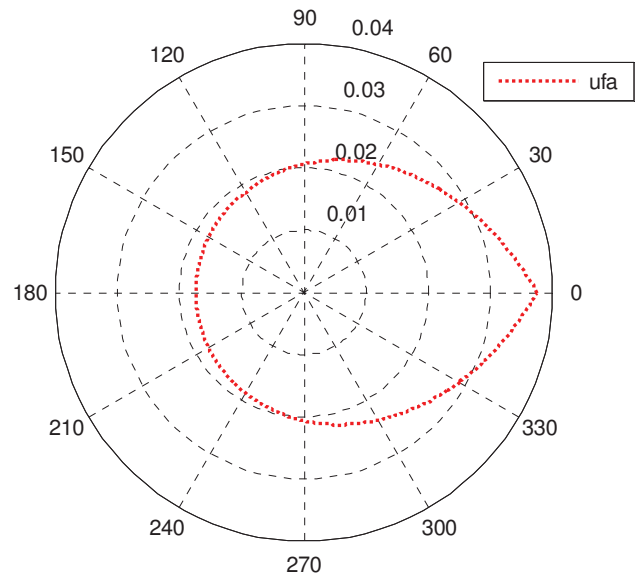was revisited for increasing the intelligibility of the method used. Uniform currents and uniform scattered fields were obtained using PO method. PO integral was converted to the series form using the Hankel functions, which are the combination of the solution of Bessel's equation. Then to take into account the known exact scattered field from the cylinder, the contribution of the non-uniform current to the scattered field was obtained using the PTD method. In this thesis, the PO integral was converted to a series solution because its conversion is much easier than the conversion of the total exact scattered field from the series form to the integral form. In addition, the non-uniform scattering field can be found from the integration of the fringe current but it is too complex to evaluate the exact current over the surface of the scatterer. Moreover, we investigated the scattered and the diffracted fields from an impedance cylinder with the method of the PTD. Although the PO scattered field includes the edge diffraction it gives wrong values. Total field includes total surface diffraction and total reflected fields. The difference between the total field and the PO field is fixed by the non-uniform field. Surface diffractions and non-uniform current's contribution to the scattered field were investigated numerically. The benefit of this theory is fixing the defects of the PO methods in the diffraction part for curved impedance surfaces, which do not exist in the literature. It is possible to investigate the complex geometries like parabolic, hyperbolic or ellipsoidal surfaces using these fringe currents. It is seen that the contributions of the non-uniform parts are not negligible for scattering.

In addition, in this thesis scattering surface integrals were reduced to the line integrals for investigation of the exact diffracted fields. Hence this formulation was generalized for various diffraction applications. This formulation is based on the MTPO axioms. In contrary to the other approaches, this derived expression is based on the MTPO axioms and scattering angle is variable at the corners and the edges. This is the main advantageous of this approach. This new formulation was applied on the PEC cylindrical parabolic reflector geometry, which was fed by the H-polarized line source. The PO diffracted fields were found. Fringe field's expressions were derived. The asymptotic evaluations of the diffraction integrals lead to the fringe fields. The fringe fields were used for fixing the PO diffracted fields and the exact diffracted fields were obtained. The PO, the fringe and the exact diffracted fields were analyzed numerically. The exact diffracted fields were investigated numerically for different incident angles. It is observed that the results are in the harmony with the theory.

Furthermore, uniform and asymptotic fringe field expressions were derived for a half plane with the impedance boundary conditions by using the method of PTD. First of all, the contributions of the PO fields were derived by integrating the fields in the given surface. Then, the field expression, which had been obtained from the surface integral was subtracted from the exact solution in order to obtain the asymptotic form of the fringe fields. The asymptotic fringe fields were transformed into the uniform fringe fields by using the method which is given in Refs. [58-59].

The derived uniform fringe fields were found to be more reliable than the asymptotic forms because asymptotic expressions give wrong field values in the transition regions. It was observed that the separated fringe fields compensate the reflected and incident fields in the shadow regions. Numerical analysis showed that the uniform fringe fields are in harmony with the theory. We observed that amplitudes of the asymptotic fringe field are finite for all direction of observation and nearly consistent with the uniform fringe fields except for the reflection and shadow boundaries. In this respect, when compared to Ufimtsev's works, it appears that Ufimtsev's amplitude values were exaggerated [5-62]. In chapter 4, Fig. 4.2 of Ref. [5], amplitude values of asymptotic fringe field components take equal value with GO fields [5]. However, it is noticeable that diffracted fields amplitude values have to be

half of the GO amplitude values in the shadow and reflection regions. The more rigorous expressions were presented and numerically analyzed in this thesis.

REFERENCES

1. **Balanis C. A.**, **(1989),** "*Advanced Engineering Electromagnetics*", Wiley, New York.

2. **Keller J. B.**, **(1962),** "*Geometrical Theory of Diffraction*", J.Opt.Soc.Am., vol. 52, pp.116-130.

3. **Kouyoumjian R. G. and Pathak P. H.**, **(1974)**, "*A Uniform Theory of Diffraction for Edge in A Perfectly Conducting Surface*", Prog. IEEE, vol.62 no. 11, pp. 1448-1461.

4. **McDonald H. M., (1913),** "*The Effect Produced by An Obstacle on A Train of Electric Waves*", Phil. Trans. R. Soc. Lond., Ser. A., Math. Phys. Sc., vol. 212, pp. 299-337.

5. **Ufimtsev P. Ya.**, **(2007),** "*Fundamentals of The Physical Theory of Diffraction*", Wiley, New Jersey.

6. **Ufimtsev P. Ya., (1989),** "*Theory of Acoustical Edge Waves*", J. Acoust. Soc. Am., vol. 86, pp. 463-474.

7. **Ufimtsev P. Ya., (2007),** "*Fast Convergent Integrals for Nonunifrom Currents on Wedge Faces*", J. Electromagnetics, vol. 18, pp. 289-313.

8. **Ufimtsev P. Ya., (1991),** "*Elementary Edge Waves and The Physical Theory of Diffraction*", J. Electromagnetics, vol. 11, pp. 125-160.

9. **Ufimtsev P. Ya., (2006),** "*Improved Theory of Acoustic Elementary Edge Waves*", J. Acoust. Soc. Am, vol. 120, p. 631.

10. **Ufimtsev P. Ya., (2006),** "*Improved Physical Theory of Diffraction: Removal of the Grazing Singularities*", IEEE Trans. Antennas Propogat., vol. 54, pp. 2698-2702.

11. **Umul Y. Z., (2004),** "*Modified Theory of Physical Optics,*" Opt. Express, vol.12, no. 20, pp.4959–4972.

12. **Pathak P., (1979),** "*An Asymptotic Analysis of The Scattering of Plane Waves by A Smooth Convex Cylinder*", Radio.Sci., vol.14, pp. 419-435.

13. **Franz W., (1954),**" *Über die Green'she Funktion des Zylinders und der Kugel*", Z. Naturforsch., vol. 9a, pp.705-716.

14. **Borghi F., Santarsiero M., Frezza F., Schettini G., (1996),** "*Plane-wave Scattering by A Perfectly Conducting Circular Cylinder Near A Plane Wave Surface: Cylindrical-Wave Approach*", J. Opt. Soc. Am., vol. 13, pp. 483-493.

15. **Kouyoumjian R. G., (1965),** "*Asymptotic High-Frequency Methods*", Proc. IEEE, vol.53, pp.864-876.

16. **Keller J. B., (1956),** "*Diffraction by A Convex Cylinder*", IRE. Trans. on Antennas and Propagation, vol. AP-4, pp. 312-321.

17. **Rayliigh L., (1881),** "*On The Electromagnetic Theory of Light*", Phill. Mag. (GB), vol.12, pp. 81-101.

18. **Epstein P. S., (1914),** "*Ph.D. Dissertation*", Munich, Germany.

19. **Debye P., (1908),** " *Das Electromagnetisch Feld um einen Zylinder und Die Theorie des Regenbogens*", Phys. Z., vol.9, pp.775-779.

20. **Riblet H. J., (1959),** "*Second Order Geometric Optic Currents on A Cylinder*", in Proc.McGill Symp. On Microwave Optics, pt. II Bedford, Mass.: Electronics Research Directorate, AF Cambridge Research Center, pp. 215-225.

21. **Wetzel L.**, **(1957),** " *High Frequency Current Distributions on Conducting Obstacles*", Cruft Lab., Harvard University, Cambridge, Mass., Scientific Rept. 10, Contract AF 19, pp.604-786.

22. **Waith J. R.**, **(1959),** "*Electromagnetic Radiation from Cylindrical Structures*", Pergamon, New York, Based on NBS Rept. 5553, 1958.

23. **Lawrence D. E., Sarabandi K.**, **(2002),** "*Electromagnetic Scattering from A Dielectric Cylinder Buried Beneath A Slightly Rough Surface*", IEEE Trans Antennas and Propogation , vol. 50, no. 10.

24. **Yalçın U.**, **(2007),** "*Scattering from A Cylindrical Reflector: Modified Theory of Physical Optics Solution*", J. Opt. Soc. Am. A., vol. 24, no.2, pp.502-506.

25. **Umul Y. Z., Yengel E., Aydın A.**, **(2003),** " *Comparision of Physical Optics Integral and Exact Solution for Cylinder Problem*", in Proceedings of ELECO 2003, Third International Conference on Electrical and Electronics Engineering, Bursa, Turkey, pp.245-248, 31-34.

26. **Borghi R., Gori F., Santarsiero M., Frezza F., Schettini G., (1996),** " *Plane Wave Scattering by A Perfectly Conducting Circular Cylinder Near A Plane Surface: Cylindrical-Wave Approach*", J. Opt. Soc. Am. A., vol. 13, no.3, pp.483-493.

27. **Büyükaksoy A., Uzgören G.**, **(1988),** "*Diffraction of High Frequency Waves by A Cylindrically Curved Surface with Different Face Impedance*", IEEE Transactions on Antennas and Propagation, vol. 36, no.5, pp.592-600.

28. **Michaeli A., (1993),** "*Application of Physical Optics and Physical Theory of Diffraction to A Smooth Convex Surface*", J. Electromagnetic Waves App., vol. 7, pp. 1623-1631.

29. **Syed H. H., Volakis J. L., (1996),** "*PTD Analysis of Impedance Structures*", IEEE Trans. Antennas Propogat., vol. 7, pp. 983-988.

30. **Başdemir H. D., (2010),** M.S. Thesis, Dept. of Elec. Comm. Eng., Çankaya Univ., Turkey.

31. **Başdemir H. D. (2011),** "*Non-uniform Currents Flowing on A Perfectly Conducting Cylinder*", In General Assembly and Scientific Symposium XXXth URSI, IEEE, pp. 1-4.

32. **Rubinowicz A., (1957),** "*Thomas Young and the Theory of Diffraction*", Nature, vol. 180, pp. 4-162.

33. **Maggi G.A., (1888),** "*Sulla Propagazione Libre e Perturbata Delle Onde Luminose in un Mezzo Izotropo*", Ann. Mat., vol. 16, pp. 21-48.

34. **Rubinowicz A., (1917),** "*Die Beugungswelle in der Kirchoffschen Theorie der Beugungsercheinungen*", Ann. Phys., vol. 4, pp. 78-257.

35. **Ganci S., (1995),** "*A General Scalar Solution for The Half-Plane Problem*", J. Mod. Opt., vol. 42, pp. 11-1707.

36. **Ganci S., (1996),** "*Half Plane Diffraction in Case of Oblique Incidence*", J. Mod. Opt., vol. 43, pp. 51-2543.

37. **Ufimtsev P. Ya., (1971),** "*Method of Edge Waves in The Physical Theory of Diffraction*", Air force system command, foreign tech. div. document ID No. FTD-HC-23-259-71 (Translation from the Russian version published by Soviet Radio House, Moscow, 1962).

38. **Mitzner K. M., (1974),** "*Incremental Length Diffraction Coefficients*", Aircraft Division Northrop Corp., Tech. Rep. No. AFAL-TR-73-296.

39. **Michaeli A., (1984),** "*Equivalent Edge Currents for Arbitrary Aspects of Observation*" IEEE Trans. Antennas. Propogat., AP-32, pp. 252-258.

40. **Knott E. F., (1985),** "*The Relationship between Mitzner's ILTS and Michaelie's Equivalent Currents*", IEEE Trans. Antennas. Propogat., AP-33, pp. 112-114.

41. **Umul Y. Z., (2008),** "*MTPO Based Potential Function of the Boundary Diffraction Wave Theory*", Opt. Laser Tech., vol. 40, pp. 769-774.

42. **Umul Y. Z., (2009)**, "*Rigorous Expressions for The Equivalent Edge Currents*", Progress in Electromagnetic Research B., vol. 15, pp. 77-94.

43. **Büyükaksoy A., Uzgören G., (1987)**, "*High-Frequency Scattering from The Impedance Discontinuity on A Cylindrical Curved Impedance Strip*", IEEE Trans. Antennas. Propogat., vol. 35, pp. 234-236.

44. **Akduman I., Büyükaksoy A., (1995)**, "*Asyyptotic Expressions for The Surface Currents Induced on A Cylindrically Curved Impedance Strip*", IEEE Trans. Antennas. Propogat., vol. 43, pp. 453-463.

45. **Umul Y. Z., (2008)**, "*Scattering of A Line Source by A Cylindrical Parabolic Impedance Surface*", J. Opt. Soc. A., vol. 25, pp. 1652-1659.

46. **Yalçın U., Sarnik M. (2013)**, "*Uniform Diffracted Fields from A Cylindrical Reflector with Modified Theory of Physical Optics*", The Sci. Word J., vol. 2013, pp. 1-6.

47. **Umul Y. Z., (2008)**, "*Fringe Waves Radiated by A Half-Plane for The Boundary Conditions of Neumann*", App. Phys. B., vol. 93, 885-889.

48. **Syed H., Volakis J. L., (1996)**, "*PTD Analysis of Impedance Structures*", IEEE Trans. Antennas. Propogat., vol. 44, pp. 983-988.

49. **Casciato M. D., Sarabandi K., (2001)**, "*Scattering from A Land-Sea Transation*", IEEE Antennas Propogat. Symp., vol. 1, pp. 452-455.

50. **Casciato M. D., (2001)**, "*Radio Wave Diffraction and Scattering Models for Wireless Channel Simulations*", Ph.D. Thesis. , Univ. of Michigan.

51. **Corona P., D'Ambrosio G., Franceschetti G., (1979)**, "*Scattering Properties of Satellite-Borne Solar Cell Panels*", IEEE Trans. Antennas. Propogat., vol. 27, pp. 496-499.

52. **Bucci O. M., Francesschetti G., (1976)**, "*Electromagnetic Scattering by A Half-Plane with Two Face Impedance*", Radio. Sci., vol. 11, pp. 49-59.

53. **Umul Y. Z., (2005),** "*Modified Theory of Physical Optics Approach to Wedge Diffraction Problems*", Opt. Exp., vol. 13, pp. 216-224.

54. **Sommerfeld A., (1896),** "*Mathematische Theorie der Diffraction,*" Math. Ann., vol. 47, pp.317–374

55. **Young T., (1802),** ,"The *Bakerian Lecture: On The Theory of Light and Colours,*" Phil. Trans. R. Soc. London, vol. 92, pp.12-48.

56. **Harrington R.F., (2001),** "*Time-Harmonic Electromagnetic Fields*", Wiley, New York, IEE Press Series on Electromagnetic Wave Theory.

57. **Stutzman W. L., Thiele G. A., (1998),** Antenna Theory and Design, Wiley, New York.

58. **Umul Y. Z., (2008),** "*Uniform Version of The Modified Theory of Physical Optics Based Boundary Diffraction Wave Theory*", J. Mod. Opt., vol. 55, pp. 2797-2804.

59. **Umul Y. Z., (2008),** "*Uniform Theory of The Boundary Diffraction Wave*", Opt. Laser Tech., vol. 41, pp. 285-288.

60. **Umul Y. Z., (2011),** "*Physical Optics Theory for The Diffraction of Waves by Impedance Surfaces*", J. Opt. Soc. Am. A, vol. 28, pp. 255-262.

61. **Maliuzhinetz, G. D., (1960),** "*Das Sommerfeldsche Integral und die Lösung von Beugungsaufgaben in Winkelgebieten*", Ann. Phys. vol. 461, pp. 107-112.

62. **Hacıvelioğlu F., Sevgi L., Ufimtsev, P. Ya., (2011),** "*Electromagnetic Wave Scattering from A Wedge with Perfectly Reflecting Boundaries: Analysis of Asymptotic Techniques*", IEEE Antennas Propogat. Mag., vol. 53, pp. 232-253.

CURRICULUM VITAE

PERSONAL INFORMATION
Surname, Name: Başdemir, Hüsnü Deniz
Date and Place of Birth: 1 April 1985, Doğanhisar
Marital Status: Single
Phone: +90 543 336 16 35
Email: basdemir@cankaya.edu.tr

EDUCATION

Degree	Institution	Year of Graduation
M.Sc.	Çankaya Univ., Elec. and Comm. Engineering	2010
B.Sc.	Çankaya Univ., Elec. and Comm. Engineering	2008
High School	Akşehir Anatolian Teacher High School	2003

WORK EXPERIENCE

Year	Place	Enrollment
2009- Present	Çankaya Univ. Department of Electronic and Communication Engineering	Specialist
2007 July	Türk Telecom.	Trainer
2006 July	Ortana Co.	Trainer

FOREIN LANGUAGES
Advanced English, Beginner French

PUBLICATIONS

1. Başdemir, H. D., "*Fringe Waves in An Impedance Half-Plane*", Progress in Electromagnetic Research, vol. 138, pp. 571-584, (2013).

2. Başdemir, H. D., "*Impedance Surface Diffraction Analysis for A Strip with the Boundary Diffraction Wave Theory*", Optik, Int. J. Light Electron. Opt., vol. 124, pp. 627-630, (2013).

3. Başdemir, H. D., "*Fringe Waves on An Impedance Cylinder*", Optik, Int. J. Light Electron. Opt., vol. 124, pp. 4999-5002, (2013).

4. Basdemir, H. D. "*Nonuniform Currents Flowing on A Perfectly Conducting Cylinder.*" General Assembly and Scientific Symposium, 2011 XXXth URSI. IEEE, (2011).

5. Başdemir, H.D., "*Silindirik Reflektörden Saçılan Alanların Sınır Kırınım Teorisi ile İncelenmesi*", 4. Mühendislik ve Teknoloji Sempozyumu Bildiriler Kitabı, Çankaya Üniversitesi, 284-288, Ankara, (2011).

6. Amidi M, Başdemir D. ve Umul Y. Z., "*Sonlu Dalga Kılavuzundan Elektromanyetik Dalgaların Saçılması*", 3. Mühendislik ve Teknoloji Sempozyumu Bildiriler Kitabı, Çankaya Üniversitesi, 381-387, Ankara, (2010).

7. Başdemir H. D. ve Umul Y. Z., "*Düzlemsel Dalgaların Dirichlet ve Neumann Koşullarına Sahip Yüzeylerden Oluşmuş Yarım Düzlemden Kırınımı*", 2. Mühendislik ve Teknoloji Sempozyumu Bildiriler Kitabı, Çankaya Üniversitesi, 71-76, Ankara, (2009).

REVIEWED BOOKS

1. Fundamentals of the Physical Theory of Diffraction by Pyotr Ya. Ufimtsev, New York, Wiley/IEEE Press, 2007, 329 pp., ISBN: 9780470097717, reviewed for Radio Scientists Bulletin, March 2013.

PROJECTS

1. Smart Mobile Antenna, Project Number: 0934.TGSD.2014, Ministry of Science, Industry and Technology, 2014.

HONOURS AND AWARDS

1. Young Scientists Award 2011
   International Union of Radio Science (URSI)
2. Graduate Honor Student 2008
   Çankaya University

HOBBIES
Chess, Puzzle, Books, Swimming, Fitness